Biophysical Mechanism for Neural Spiking Dynamics

by

Adrian Nicholas Smith

A Dissertation Presented in Partial Fulfillment
of the Requirements for the Degree
Doctor of Philosophy

Approved December 2015 by the
Graduate Supervisory Committee:

Carlos Castillo-Chávez, Co-chair
Irina Sinakevitch, Co-chair
Brian Smith

ARIZONA STATE UNIVERSITY

May 2016

ABSTRACT

In the honey bee antennal lobe, uniglomerular projection neurons (uPNs) transiently spike to odour sensory stimuli with odour-specific response latencies, i.e., delays to first spike after odour stimulation onset. Recent calcium imaging studies show that the spatio-temporal response profile of the activated uPNs are dynamic and changes as a result of associative conditioning, facilitating odour-detection of learned odours. Moreover, odour-representation in the antennal lobe undergo reward-mediated plasticity processes that increase response delay variations in the activated ensemble of uniglomerular projection neurons. Octopamine is necessarily involved in these plasticity processes. Yet, the cellular mechanisms are not well understood. I hypothesize that octopamine modulates cholinergic transmission to uPNs by triggering translation and upregulation of nicotinic receptors, which are more permeable to calcium. Consequently, this increased calcium-influx signals transcription factors that upregulate potassium channels in the dendritic cortex of glomeruli, similar to synaptic plasticity mechanisms recently shown in various insect species. A biophysical model of the antennal lobe circuit is developed in order to test the hypothesis that increased potassium channel expression in uPNs mediate response delays to first spike, dynamically tuning odour-representations to facilitate odour-detection of learned odours.

TABLE OF CONTENTS

LIST OF TABLES

Table Page

LIST OF FIGURES

Chapter 1

INTRODUCTION

In the insect olfactory pathways, uniglomerular projection neurons (uPNs) transiently synchronize their spiking activity upon odor stimulation. Recently, immunostaining studies with dye injection into the antennal lobe (AL) reveal that some uPNs potentially share common excitatory presynaptic input from olfactory receptor neurons (ORNs), i.e., a single ORN axon collateral branches to form synaptic connections with multiple neurons. Each uPN is innervated by potentially hundreds of both common and uncommon ORN axon collaterals. During odor processing, uPNs get recruited to participate in the orquestration of the AL network activity to form neural representations of odor information. How the AL neural network coordinates the activities of uPNs during odor processing remains an area of intense research. The following paragraphs outline research aimed toward creating a theoretical framework that allows translation of measures of synchronized spiking into plausible renditions of synaptic connectivity.

In honey bee, the olfactory sensory network begins with olfactory receptor neurons (ORNs) projecting their axons onto antennal lobe glomeruli in a receptor-specific manner (*Laissue and Vosshall, 2008*). The ORNs are input neurons that relay odor information to uniglomerular projection neurons (uPNs) and local interneurons (LNs) in the cortex area of glomerulus (*Fonta et al., 1993; Hummel and Zipursky, 2004; Tanaka et al., 2012a*). The LNs form synaptic connections that are strictly confined to the antennal lobe (*Schafer and Bicker, 1986; Fonta et al., 1993; Olsen et al., 2007b; Shang et al., 2007; Seki et al., 2010; Meyer and Galizia, 2012; Girardin et al., 2013*). The uPNs are output neurons that extend their axon collaterals outside the antennal lobe to the mushroom body and lateral protocerebrum neuropils (*Galizia and Rssler, 2010; Stocker et al., 1990; Fonta et al., 1993; Abel et al., 2001; Kirschner et al., 2006; Tanaka et al., 2008, 2012a*). The intrinsic neurons of the mushroom bodies (Kenyon cells) decode olfactory sensory information by detecting coincident or synchronized input from uPNs (*Krofczik et al., 2008*).

Previous studies have investigated the *in vivo* stimulus-response dynamics of individual uPN spiking activity, where odor stimulation was typically applied in durations lasting a couple of seconds (*Nawrot, 2010*). During the first 300-600 milliseconds (*ms*) of odor presentation, intracellular

recordings show an initial increase in the spiking rate of activated uPNs, followed by a rate decrease. The spiking stabilizes, reaching a constant firing rate, and remains at this spiking frequency despite odor being continuously applied (*Nawrot, 2010*). This so called *phasic-tonic* odor-response characteristic of uPN spiking dynamics has been shown in both insect and mammalian olfactory systems (*Krofczik et al., 2008*). Furthermore, a subset of the these uPN ensembles temporarily display significant spiking synchronization, i.e., only a fraction of the spikes from such neurons occur within a few milliseconds of one another. Moreover, the number of synchronized spikes is more than would be predicted if the neurons fired independently.

A minimal model is used with minimal number of equations of neuronal membrane potential while using biophysical variables to describe membrane potential. In addition, the model considers realistic excitatory synaptic input based on kinetics of synaptic transmission. To test the hypothesis, the model considers two layers of neurons, where we assume ORNs form the input layer and uPNs form the output layer. Here, the output layer consists of two uncoupled uPNs, whose membrane potential dynamics were derived using dynamical systems theory. The input layer consists of hundreds of ORNs, whose excitatory synaptic input are modeled as stochastic renewal processes. The model uPNs should be uncoupled to control for the possibility of synchronized spiking resulting from direct or indirect synaptic connections. Results from this research will be part of a dissertation to obtain a doctoral degree in Applied Mathematics for the Life and Social Sciences.

Chapter 2

LITERATURE REVIEW

2.1 Neuroanatomy of Olfactory Pathways in Honey Bee

Using honey bees as a model, the following paragraphs contain a brief overview of the organization of the olfactory neural networks, all relative to the spiking activity of projection neurons (PNs) and how it can be used to make inferences about the synaptic organization of excitatory inputs to PNs.

Odor processing involves the orchestration of multiple layers of neural networks that detect odor molecules in the environment and rapidly encode and discriminate among distinct odors (*Fonta et al., 1993; Abel et al., 2001; Strausfeld, 2002; Sinakevitch et al., 2005, 2011; Kelber et al., 2006; Kirschner et al., 2006; Schrter et al., 2007; Girardin et al., 2013*). A recent study in honey bees has demonstrated their ability to distinguish between different olfactory stimuli that are as short as 200 ms (*Wright et al., 2009*). Behavioral experiments show that honey bees can learn to discriminate odors in less than 200 milliseconds (*Wright et al., 2009; Fernandez et al., 2009*). Additionally, mice are able to discriminate dissimilar odors within < 250 *ms* (*Abraham et al., 2004*) Olfactory path-

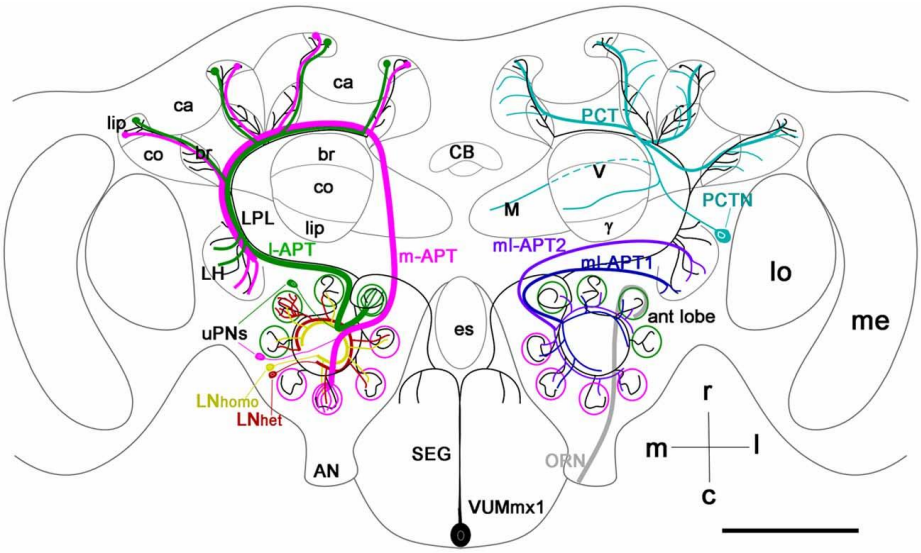

Figure 2.1: Schematic of Olfactory Neural Networks in Honey Bee

ways begin with odor molecules triggering a signal transduction process, where receptor proteins expressed in olfactory receptor neurons (ORNs) protrude through pore plate sensilla of the anten-

nae and bind to odor molecules (*Krofczik et al., 2008*). ORNs detect and respond to odor molecules from the environment and relay this information via four antennal nerve tracts (T1-T4) (*Kirschner et al., 2006*).

These nerve tracts are comprised of an estimated 65,000 ORNs that input to the antennal lobe (AL) neural network (*Esslen and Kaissling, 1976*). The AL is comprised of 160 neuropil structures called glomeruli, shaped by the synaptic connectivity of different types of neurons, which were revealed by detailed anatomical studies in tissue (*Arnold et al., 1985; Flanagan and Mercer, 1989; Kelber et al., 2006; Sachse, 2002*). The neurons revealed in these studies include ORNs, uni- and multi-glomerular projection neurons (uPNs, and mPNs), and local GABAergic inhibitory interneurons (LNs) (*Galizia et al., 1999; Robertson and Wanner, 2006; Sinakevitch and Smith et al., 2013*) (See Figure 2.2).

2.2 Projection Neurons and Associated Synaptic Inputs

Anatomically we distinguish two types of uPNs (*Abel et al., 2001; Kelber et al., 2006; Kirschner et al., 2006; Nishino et al., 2009*). There are an estimated 920 total uPNs in the AL as reported by Rybak (2012). The lateral PNs (l-PNs) receive input exclusively from T1 glomeruli and send their axons along the lateral antennocerebralis tract to the higher order brain centers, the lateral horn (LH) and the MB. The median PNs (m-PNs) exclusively originate in T2-4 glomeruli and project along the median antennocerebralis tract, first to the MB and then to the LH (*Abel et al., 2001; Bicker et al., 1993; Kirschner et al., 2006; Mobbs, 1982; Mller et al., 2002*). The LNs form inhibitory interconnections between the glomeruli, with synaptic connections strictly confined to AL circuitry (*Schafer and Bicker, 1986; Fonta et al., 1993; Olsen et al., 2007b; Shang et al., 2007; Seki et al., 2010; Meyer and Galizia, 2012; Girardin et al., 2013*). In contrast, uPNs branch their axon collaterals outside the AL to form presynaptic input to higher-order brain centers of the olfactory pathways, which include areas of the brain that process and integrate multiple sensory modalites.

2.3 Olfactory Receptor Neurons

Each individual glomerulus receives input only from ORNs that express the same chemical receptor protein (*Laissue and Vosshall, 2008*). Even though these ORNs may originate from different regions distributed over the entire antennae, their axon collaterals eventually converge and terminate

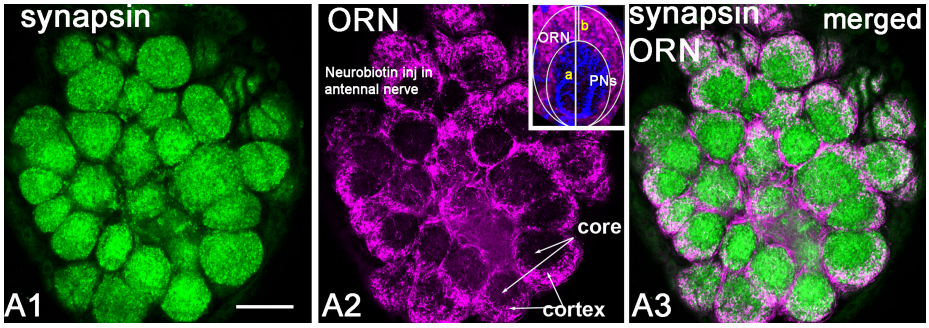

Figure 2.2: Neuroanatomy and Synaptic Structure of the Antennal Lobe

in one specific glomerulus (*Vosshall et al., 2000*). Thus, activation of a single glomerulus reflects the chemoprofile of the respective receptor type, and the glomerular activation pattern reflects the combination of activated receptor types.

Individual glomerulus have layers of synaptic connections that form a characteristic outer cortex and inner core area (*Fonta et al., 1993; Hummel and Zipursky, 2004; Tanaka et al., 2012a*). Each glomeruli contains 5-6 uniglomerular projection neurons (uPNs) that have dendritic branching in both the cortex and core areas of only one glomerulus, hence the term *uniglomerular*. The uPNs have thicker branchings in the core and very thin dendritic ramifications in the cortex of glomeruli. Indirect evidence suggests these thin uPN dendrites receive excitatory presynaptic input from ORNs in the glomerular cortex, where these experimental studies show that ORN synapses are virtually absent in the core area of glomeruli. In the glomerular core layer, uPNs mainly receive GABAergic inhibitory synapses from LNs. Next, the uPNs extend their axon collaterals outside the AL, forming presynaptic input to higher-order neuropils such as the mushroom bodies and the lateral protocerebral lobes (*Esslen and Kaissling*, 1976).

Within each glomeruli, the uPNs integrate synaptic input received from thousands of input neurons in the AL circuitry, which drive both excitation and inhibition processes mediated by fast ligand-gated ion channels. The uPNs process and transform this bombardment of synaptic signals and not just passively relaying odor information received from AL network.

2.4 Synaptic Plasticity Processes Via Octopamine and Tyramine

In the honey bee antennal lobe (AL), uniglomerular projection neurons (uPNs) transiently spike to odour sensory stimuli with odour-specific response latencies, i.e. delay to first spike after odour stimulation onset (*Krofczik, Menzel et al, 2009*). Recent Ca^{2+} imaging studies show that the spatio-temporal response profile of the activated uPN ensemble is dynamic and changes as a result of associative conditioning, facilitating odour detection of learned odours (*Fernandez et al, 2009*). Therefore, we propose odour-representation in the AL undergo reward-mediated plasticity processes that increase response delay variations in the activated uPN ensemble. Octopamine (OA) is necessarily involved in these plasticity processes, yet the cellular mechanisms are not well understood. We propose that OA modulates cholinergic transmission to uPNs by triggering translation and upregulation of $\alpha 7$ nicotinic receptors, which are more permeable to Ca^{2+}. Consequently, this increased Ca^{2+}-influx from $\alpha 7$ signals transcription factors that upregulate *Shal*-type K^+ channels in the dendritic cortex of glomeruli, similar to synaptic plasticity mechanisms recently shown in *Drosophila* (*Ping and Tsunoda, 2012*). We develop a biophysical model of the AL circuit to test the hypothesis that increased *Shal* expression in uPNs mediate response delays to first spike, dynamically tuning odour-representations to facilitate odour detection of learned odours.

2.5 Functional Properties of Cholinergic Receptors

Reference numbers are from (Saragoza 2003):

- α-bungarotoxin-sensitive. Have high affinity with $\alpha 7$[15,53,54]
- highly permeable to calcium[15,53,54]
- mammalian $\alpha 7$ nAChRs are homo-oligomers; most abundantly expressed in the hippocampus[10,19]
- found in presyanptic, postsynaptic, and nonsynaptic processes[22,56]
- mediate GABAergic transmission[2,24,36]
- modulate glutamate release[37,43,51]
- modulate dopamine secretion from nucleus accumbens[25]

- influence spatial and working memory[23,39]
- activation can enhance LTP and LTD in hippocampus[40]
- induces LTP in ventral tegmental area[40]
- involved in developmental processes, e.g. neurite outgrowth[8,13,47]

Alternative RNA Processing of Cholinergic Receptor Subunits

Recent studies of *Drosophila* uPNs show that $\alpha 7$ is upregulated 3-5 minutes after recovery from a 24 hour treatment with curare, which bind to and inactivate nAChRs (*Ping and Tsunoda, 2012*). Therefore, prolonged receptor inactivity triggered a homeostatic plasticity response to replace disfunctional receptors. We propose that OA serves as a functional analog to curare, inducing prolonged nAChR-inactivation, via post-transcriptional modifications to $\alpha 7$ subunits that diable receptor function. splice variants, resulting from β-adrenergic-like OA receptor activation. OA mediates fast $\alpha 7$ desensitization by triggering production of truncated $\alpha 7$ splice variants.
Main finding from (*Saragoza, 2003*):

- Splice variant of $\alpha 7$ subunit functions as a dominant-negative effecter of normal $\alpha 7$ subunit function
- Splice variants assemble with normal $\alpha 7$ subunits, acting as a negative regulator

Main finding from (*Cassaenaer and Laurent, 2012*):

- OA appilcation to the MBs modulate specifically the KC-β-LN synapses that previously underwent STDP LTP processes during odour presentation.
- OA modification resulted in depressed synaptic input, reversing LTP to LTD

This recent study provides evidence to support our prosal for that a major role of octopaminergic synaptic modulation is to induce a homeostatic synaptic plasticity response to prolonged receptor inactivity by mediating a fast synaptic receptor desensitization process. Octopamine (OA) induces a cAMP-dependent plasticity process in uPNs via β-adrenergic-like receptors. These receptors signal cAMP production that trigger post-transcriptional modifications amounting to a *negative allosteric*

effect on $\alpha 7$ subunit function. Moreover, this dominant-negative effecter of normal $\alpha 7$ subunit function triggers a homeostatic synaptic plasticity process that leads to upregulation of normal $\alpha 7$ RNA transcripts. A similar case has been documented in *Drosophila* (*Ping and Tsunoda, 2012*).

Specific plasticity process: β-adrenergic-like OA receptor activation leads to post-transcriptional modifications that truncate normal $\alpha 7$ protein synthesis. These truncated splice variants assemble with normal $\alpha 7$ subunits and desensitize receptor function, leading to a depressed Ca^{2+} influx. Studies of the mammalian neuromuscular junction show a neuropeptide mediating fast desensitization of nAChRs. Although the physiological significance of this fast receptor desensitization is unknown, prolonged receptor inactivity could trigger a general homeostatic response to replace disfunctional receptors. For example, receptors rendered disfunctional from natural "wear-and-tear" expected after prolonged use. Moreover, they show that $\alpha 7$ expression is necessary to induce transcription of a gene encoding a specific A-type (transient) K^+ channel, namely *Shal/Kv4*. This transient voltage-gated channel is kinetically distinct from other transient K^+ channels due to lower voltage-dependency for inactivation.

Chapter 3

DYNAMICAL NEURAL PLASTICITY IN HONEY BEE

3.1 Octopamine and Tyramine Metabolic Synthesis

Octopamine and tyramine are biogenic monoamines endogenous to invertebrates, implicated in important regulatory and modulatory roles of behavior (*Roeder, 1999; Scheiner, 2006*). Octopamine (OA), β*,4-dihydroxyphenethylamine*, is synthesized from tyramine (TA), *4-hydroxy- phenethylamine*, by tyramine β-hydroxylase. TA and the catecolamines (norepinephrine, epinephrine and dopamine) are all synthesized from the amino acid tyrosine. OA shares similar molecular structure with norepinephrine, a vertebrate biogenic amine that has not been found in invertebrate physiology. The table below displays two different OA and TA metabolic synthesis pathways.

OA and TA trigger intracellular signaling pathways by binding with different affinities to oc-

Pathway[1]	Tyrosine → Tyramine → Octopamine
Pathway[2]	Tyrosine → L-DOPA → Dopamine → Tyramine → Octopamine
[1] is the common OA synthesis pathway (*Roeder, 1999*)	

Figure 3.1: Octopamine and Tyramine Metabolic Synthesis

topamine receptors (OARs) or tyramine receptors (TYRs), which are known to be G-protein coupled receptors (GPCRs). GPRCs are referred to as seven-transmembrane proteins with an extracellular N-terminus and intracellular C-terminus. The N-terminus domain binds the ligand, e.g. OA or TA, whereas the C-terminus binds secondary messengers at the intracellular c-loop domain. (*Blenau 2000; Grohmann 2003*). In addition, the intracellular signaling pathways triggered by OARs and TARs follow classic second messenger cascades during signal transduction.

In Honey bee, 19 GPCR genes have been identified including receptor genes for octopamine, tyramine, dopamine, seratonin, and acetylcholine (*Hauser, 2006*). Among these, 4 OAR receptor genes have been identified, but only one gene has been cloned and functionally characterized, *AmOA1* (*Grohmann, 2003*). This receptor is categorized into the α-adrendergic-like receptors (αOARs), homologous to vertabrate α1-adrenergic receptor subtype, (*Grohmann, 2003*). Similarly, *AmTYR1*, is the only tyramine receptor characterized in honey bee, belonging to the tyramine receptor subtype

TYR1 (*Blenau, 2001, 2003; Mustard, 2005*). Table 1 displays octopamine and tyramine receptors identified in honey bee. Also, octopamine-like and tyramine-like receptors yet to be characterized in honey bee.

Ref. Label (*Hauser, 2006*)	Deorphanized receptor	ligand	References
Am 5	AmOA1 (α-adrenergic-like) $\uparrow [Ca^{2+}]_i$ $\uparrow$ cAMP	Octopamine	(*Grohmann 2003*) *Blenau, 1998, 2000*)
Am 7	AmTYR1 $\downarrow$ cAMP	Octopamine/ tyramine	(*Blenau, 2000*)
Orphan honey bee receptors	Data from other insects		
Am 1-4	(β-adrendergic-like) $\uparrow$ cAMP OA > TA	Octopamine-like	(*Maqueira, 2005*)
Am 13	$\uparrow [Ca^{2+}]_i$ TA only	tyramine-like	(*Huang, 2009*)
Am 10, 14, 17, 18		ligand unknown	

Figure 3.2: Octopamine and Tyramine Receptor Genes

3.2 Subcellular Signaling Pathways of Octopamine and Tyramine

OARs and TYRs are members of the GPCR superfamily which activate G-proteins (guanine nucleotide-binding proteins) of the heterotrimeric type, consisting of three subunits Gα (alpha), Gβ (beta) and Gγ (gamma). During signal transduction, OARs and TYRs are activated by binding OA or TA with different affinities. These receptors undergo a conformational change and catalyze a reaction causing G-proteins to release a bound GDP molecule in exchange for GTP. This enzymatic activation of the G-protein by GPCRs yields two active subunits, Gα-GTP and a G$\beta\gamma$ dimer complex, which further transduce intracellular metabolic signaling pathways, such as the activation of protein kinases, release of intracellular [Ca^{2+}], and effecting various other lipid metabolites (*Hille, 2001*). With the variety of resulting intracellular signals produced from GPCR/G-protein couplings, cellular effects of OA and TA become amplified and/or diversified within the cytoplasm, even distant from the plasma membrane.

Octopamine Receptor Couples to G-Protein

With OA as the agonist, α-adrenergic receptors (αOAR) couple to G_q leading to $[Ca^{2+}]$ increases (*Grohmann, 2003; Beggs, 2011*). Additionally, these αOARs have a higher affinity for OA compared to TA.

. In the classic G-protein pathway, the G_q subunit activates phospholipase C (PLC), which hydrolyzes phosphatidylinositol 4,5-bisphosphate (PIP_2) into inositol 1,4,5-trisphosphate (IP_3) and diacylglycerol (DAG). The PLC $\rightarrow$ PIP_2 $\rightarrow$ IP_3 pathway leads to IP_3 receptor activation and intracellular $[Ca^{2+}]$ release from the endoplasmic reticulum (ER). DAG and $[Ca^{2+}]_i$ together activate protein kinase C (PKC) which phosphorlates various proteins and ion channels. In addition when expressed in the HEK293 cells, *AmOA1* couples to cAMP signaling via a PLC-independent pathway (*Beggs, 2011*).

To date, β-adrenergic-like octopamine receptors (βOARs) have not been characterized in honey bee. In *Drosophila*, βOARs have been shown to increase levels of cAMP and do not give rise to an intracellular calcium release (*Evans, 2005*). In the classical cAMP pathway, G_s stimulates a membrane-bound enzyme adenylyl cyclase producing cyclic-adenosine monophosphate (cAMP), which stimulates protein kinase A (PKA).

Tyramine Receptor Couples to G-Protein

The first reported TYR, *AmTYR1*, is pharmacologically related to α2-adrenergic receptors found in vertebrates and show affinity for both octopamine and tyramine (*Blenau, 2003*). In a study by Blenau et al, *AmTYR1*-transfected human embryonic kidney 293 cells decreased cAMP by inhibiting adenylyl cyclase (AC) via a G-protein, G_i, with TA application.

3.3 Octopamine Induced Calcium Dynamics

Studies of *AmOA1*-transfected HEK cells, show octopamine (OA) triggering intracellular calcium, $[Ca^{2+}]_i$, osciallations when OA concentration exceeds 50 nanomolars (nM). Micromolar concentrations (μM) of tyramine (TA) induced delayed calcium spikes with reduced amplitudes, compared to OA (*Blenau, 2003*). Increasing OA to 100 (nM) increased oscillatory frequency, with spike transients ranging from 40-60 seconds. Further increases of OA concentration to μM levels triggered

a single Ca^{2+} transient with very slow decay to rest ($>$ 10 mins). We assume the primary effect of OA acting through *AmOA1* is to trigger IP_3-dependent $[Ca^{2+}]_i$ release from the ER, with sub-cellular pathways as proposed in Table 1. The kinetic reaction of IP_3-induced increase of $[Ca^{2+}]_i$ is formulated as in (*Tang, 1995*). The model description is outlined below with details given in the appendix:

$$\begin{cases} \dot{X} = (g_{leak} + g)(C_{avg} - X) - v_r p_1 \dfrac{X^2}{X^2 + p_2^2} \\ \dot{R_1} = -k_1[IP_3]R_1 + k_{-1}R_2 \\ \dot{R_2} = -(k_{-1} + k_2 X)R_2 + k_1[IP_3]R_1 + k_{-2}R_3 \\ \dot{R_3} = -(k_{-2} + k_3 X)R_3 + k_2 X R_2 + k_{-3}R_4 \\ \dot{R_4} = k_3 X R_3 - k_{-3}R_4 \end{cases} \tag{3.1}$$

Variable X represents Ca^{2+} concentration in μM. Variables R_{1-4} represent fractions of IP_3 receptors in four possible states, thus are dimensionaless. OA-induced Ca^{2+} release begins with OA activating *AmOA1*, triggering IP_3 production (See Table 1). This kinetic reaction is formulated as a 2-state metabotropic response as in (*Destechxe, 1994*). The concentration of IP_3 is a function of activated *AmOA1* receptors at steady-state given by:

$$[IP_3] \quad = \quad \frac{r_1[OA]}{r_2[OA] + r_3} \qquad (\mu M) \tag{3.2}$$

For our model analysis, [OA] is systematically varied to characterize how [OA] influences intracellular Ca^{2+} dynamics. The parameters r_1, r_2, and r_3 are tuned such that $[IP_3]$ is within a physiological range. IP_3 is a soluable signal that can diffuse away from the membrane to bind IP_3-sensitive receptors (IP_3Rs) expressed on the ER. The total number of IP_3Rs is assumed constant, given by R_{Total}, and equals the sum of all four possible states: unbound (R_1), bound to IP_3 (R_2), bound to a single Ca^{2+} ion (R_3), and bound to two Ca^{2+} ions (R_4- the inactived state). With this approximation, the system is reduced by rewriting R_3 in terms of R_{Total} and the other states:

$$R_3 \quad = \quad R_{Total} - R_1 - R_2 - R_4 \qquad (\mu M) \tag{3.3}$$

The system is further reduced to 2-dimensions by using quasi-steady-state approximations of R_1 and R_2, given by R_1^* and R_2^*, respectively (See appendix). Therefore, R_3 is approximated by R^*:

$$R^* \quad = \quad R_{Total} - R_1^* - R_2^* - R_4 \tag{3.4}$$

$[Ca^{2+}]_i$ dynamics after non-dimensionalizing:

$$\begin{cases} \varepsilon \dot{x} = (\alpha_1 + \alpha_2 R^*)(C_{avg} - x) - J_{efflux}(x) \\ \dot{y} = \beta_2 R^* x^2 - y \end{cases} \tag{3.5}$$

After non-dimensionalizing $x = X/C_{avg}$ and $y = R_4$, where time, t, is rescaled by $\tau = tk_{-3}$. The slower recovery variable, y represents IP_3 receptors (IP_3Rs) in the inactivated state. Inactivation occurs when IP_3Rs bind a second Ca^{2+} ion after an initial binding. Therefore, Ca^{2+} ions inhibit their own rate of infux into the cytosol at high concentrations, given by the last term of $\dot{x}$, namely $J_{efflux}(x)$:

$$J_{efflux}(x) = \frac{x^2}{(x^2 + \kappa)} \tag{3.6}$$

where,

$$\kappa = (p_2/C_{avg})^2 \tag{3.7}$$

C_{avg} is the volumetric average Ca^{2+} concentration in ER and p_2 the Michaelis constant in units of (μM). The rate of calcium influx is given by the first term of $\dot{x}$:

$$(\alpha_1 + \alpha_2 R^*)(1 - x/C_{avg}) \tag{3.8}$$

$$\alpha_1 = g_0 C_{avg}(1 + v_r)/v_r p_1 \tag{3.9}$$

$$\alpha_2 = g_1 C_{avg}(1 + v_r)/v_r p_1 \tag{3.10}$$

The leakage coefficient and channel conductance are given by g_0 and g_1, respectively. v_r is a ratio of ER to cytosol volume. p_1 is the maximum pump rate in units ($\mu M/sec$).

Chapter 4

MATHEMATICAL MODELS OF NEURAL SPIKING ACTIVITY

4.1 Overview of Models of Cellular Excitability and Dynamical Systems Theory

The physiolgical state of an excitable cell can be modeled with a minimal dynamical system expressed in generic form as:

$$\begin{aligned} \dot{v} &= f(v,w;\vec{p}), \\ \dot{w} &= g(v,w;\vec{p}), \end{aligned} \tag{4.1}$$

A minimal biophysical model of a single neuron is given by the following system, derived from first principles of electrodiffusion (*Endersen, 2000*):

$$\begin{cases} C\dot{v} &= -(I_{Na}+I_K++I_{Shal}+I_{leak}+I_{synapses}), \\ \dot{w} &= (w_\infty - w)/\tau_w, \;\; w \in \{b,s\} \end{cases} \tag{4.2}$$

where I_{Na}, I_K, I_{Shal}, and I_{leak} are components of the transmembrane current carried by sodium, persistent K^+, an inactivating *Shal*-type K^+, and a general leak current, respectively. The general form of the ionic currents is given by:

$$I_x = A_x sinh[\frac{qz_x}{2kT}(v-v_x)] \qquad (nA) \tag{4.3}$$

where A_x is the amplitude of the current (in nA), q is the elementary charge (in C), z_x is the valence of ion x, k is the Boltzmann's constant (in $\frac{mJ}{K}$), T is absolute temperature (in $Kelvin$) and v_x is the Nernst equilibrium of x. A_x can be approximated by $a_{Na}m$, where a_{Na} is a constant representing the whole-membrane maximum current. m is a variable representing the proportion of open sodium channels, taking on values between 0 and 1. As mentioned previously, we are considering voltage-gated ionic channels. This means ionic channels open or close due to changes in the membrane potential,i.e. they may activate or inactivate. If we let $(1-b)$ be the proportion of sodium channels in the inactive state, then I_{Na} becomes:

$$I_{Na} = a_{Na}m_\infty^3(v)(1-b)sinh[\frac{qz_{Na}}{2kT}(v-v_{Na})] \tag{4.4}$$

The potassium channel is persistent and doesn't inactivate:

$$I_K = a_K b^4(v)sinh[\frac{qz_K}{2kT}(v-v_K)] \tag{4.5}$$

Similarly the K^+ gate has probability n of being in the open state. $\dot{n}$ describes the rate at which the potassium gates open. The sodium gate activates instantaneously, i.e. m instantly reaches its asymptotic value for a given membrane potential, and therefore $\dot{m}$=0. τ(V) is the time constant which controls how fast the potassium gate opens, i.e. a higher τ(V) value results in slower potassium gate activation. The K^+ gating variables are of the form:

$$\dot{w} = (w_\infty - w)/\tau_w \tag{4.6}$$

where

$$w_\infty = (1 + exp[\frac{qz_w}{2kT}(v - v_w)])^{-1} \tag{4.7}$$

The time constant, τ_w is constant measured in (msec). z_w is the gating charge (in Coloumbs) and v_w is the half activation potential of voltage-gated K^+ channels. The general leak current, I_L, accounts for voltage-independent channels and electrogenic pumps. It takes the form:

$$I_L = a_L sinh[\frac{qz_L}{2kT}(v - v_L)] \tag{4.8}$$

- *Shal*-type K^+ channels are functionally distinguished from other A-type channels by their inactivation properties, exerting a delay to first spike control mechanism after odor onset, i.e. response latency

The *Shal*-type K^+ channel is transient with fast inactivation:

$$\begin{cases} I_S = a_S S sinh[\frac{qz_K}{2kT}(v - v_K)], \\ \dot{S} = (S_\infty - S)/\tau_S \end{cases} \tag{4.9}$$

Phase Plane Analysis

Neurons are considered the fundamental unit of information processing in the central nervous system (*Kandel, 1985*). Receiving thousands of excitatory and inhibitory synaptic input, neurons must compute and process this input into a specific patterned output. The patterned output of the neuron is determined by how the neuron computes and processes the synaptic input, i.e. the patterened output is determined by the neuron's neurocomputational properties. Neurocomputational properties

of these excitable cells are deteremined, in part, by spike-initiating mechanisms, i.e. the transition from resting state to spiking. How different spike-initiating mechanisms relate to the specific patterned outputs of the neuron is still not completely understood. Therefore, the purpose of this research is to constuct a theoretical framework that characterizes the response properties of neurons to realistic excitatory and inhibitory synaptic input given qualitatively different spike-initiating mechanisms.

Based on their spike-initiating mechanisms, neurons are classified as either aggregators or res-

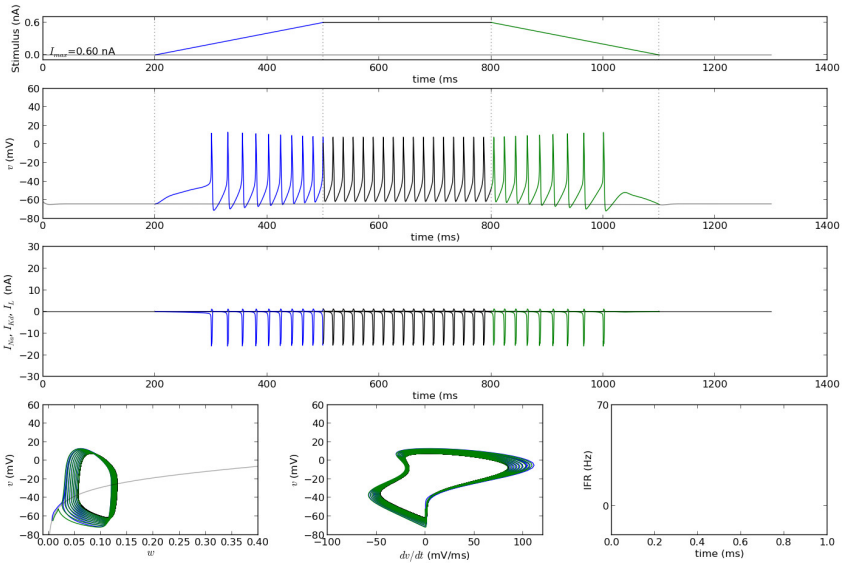

Figure 4.1: Ramp Stimulations with Externally Applied Current Source

onators. Aggregators have no preference to the frequency of synaptic input and have well defined thresholds. Resonators exhibit subthreshold oscillations and prefer synaptic input within a certain frequency band. The existence of subthreshold osciallltion is an important neurocomputational property of a neuron which confers many other processing capabilities, such as post-inhibitory rebound spiking (*Eugene, 1997*).

4.2 Neurons as Dynamical Systems

From a dynamical systems point of view, a neuron may be characterized mathematically as an excitable system. Solutions of these mathematical systems may asymptotically approach stable attractors. These attractor states may be single equilibrium states or limit cycle attractors. The

latter means the excitable system is an oscillator regime and the system exhibits periodic solutions. Bistable excitable systems have coexisting attractor states, i.e. coexistence of resting and spiking, otherwise the systems are monostable. Transitioning from resting to spiking is uniquely determined by the bifurcation of the resting state. The existence of subthreshold oscillations divide excitable systems into aggregators and resonators. Resonators exhibit subthreshold oscillations and are near Hopf bifurcation. The steady state current-voltage relationship is monotonic. Aggregators are near saddle-node bifurcation gives a non-monotonic steady-state current-voltage relationship.

The generic expression used for all the currents in the model can be derived from the first principles of electrodiffusion (*Enderson, 2001*), taking into account not only the electric field, but also diffusion to describe of ionic flux across the membrane. Channels are assumed to be permeable to only one ion. The whole membrane current carried by a channel permeable to ion x has the functional form:

$$I_x \quad = \quad A_x \cdot sinh[z_x \gamma (v - v_x)] \tag{4.10}$$

where $\gamma = \frac{q}{2kT}$, A_x is the amplitude of the current (in nA) carried by ion x, q is the elementary charge (in C), z_x is the valence of ion x, k is the Boltzmann's constant (in $\frac{mJ}{K}$), T is absolute temperature (in *Kelvin*) and v_x is the reversal potential of x. In general, the current amplitude has the form:

$$A_x(v,w) \quad = \quad \bar{a}_x \cdot p_x \tag{4.11}$$

where $\bar{a}_x$ is a constant that represents the whole-membrane maximum current (in nA) carried by the x channels. $\bar{a}_x$ is an approximation for a more complicated expression that depends on the number of proteins in the membrane, ionic mobility, and other factors[40,42]. The variable p_x represents the proportion of open x channels, and it is typically written as a product of *gating variables*, each taking values between zero and one. A_x may also include quasi-steady state or constant approximations for some of the gating variables depending on the dynamics of the system.

The dynamics of each gating variable w are determined by an equation of the form

$$\dot{w} \quad = \quad (w_\infty - w)/\tau_w \tag{4.12}$$

where

$$w_\infty(v) \quad = \quad B(v; r_w, z_w, v_w) \quad = (w_\infty - w)/\tau_w \tag{4.13}$$

and τ_w are, respectively, the time constant and steady state functions for the gating variable w . Each gating variable has three parameters: r_w, z_w, and v_w, representing the basal rate of the gating reaction (in $1/ms$), the gating charge of the closed $\rightarrow$ open reaction (in $Coulombs$), and the potential at which the rates of opening and closing are equal (in mV), respectively. The parameter values used for the gating kinetics used here are summarized in Table 1.

A model of the form in Eqs. (4.1) is said to be biophysical if the variables and parameters of the system have biophysical meaning and can be measured experimentally. For the uPN models presented in this article, f is the sum of all the currents across the membrane, normalized by the membrane capacitance. The dynamics of the uPN model can then be written as

$$\dot{v} \quad = \quad (I - I_{Na} - I_K - I_L)/C_m \tag{4.14}$$

where C_m is the membrane capacitance, and I, I_{Na}, I_K, and I_L represent, respectively, an externally applied current, Na^+, K^+, and leak currents.

Mathematical Formulation of Ion Channels

The K^+ channels were constructed based on previously reported macroscopic biophysical properties of *Shaker*, *Shal*, *Shab*, and *Shaw* channels[17,22,37,43]. Channel recordings were only taken into consideration if the results were consistent between oocyte and neuronal expression systems, and if temperature was reported for each of the experiments. The model includes a transient Na^+ current, I_{Na}, with kinetics similar to those of Na_v1 and Na_v29 channels[23,44] with fast activation and slow inactivation. K^+ currents include a persistent K^+ current carried by *Shab* channels[17] and two A-type K^+ currents carried by *Shal* and *Shaker* channels[22,37,43]. The model also includes a leak current I_L that represents the contributions of currents carried by electrogenic pumps and other voltage-independent channels[41,45].

The rate of activation of Na^+ channels is fast and is assumed to be at steady state, so that the gating variable for Na^+ activation, $m \approx m_\infty(v)$. The kinetics for the inactivation of Na^+ channels are similar to those for the activation of *Shab* channels, represented by the gating variable b. As a consequence, the inactivation of Na^+ channels is approximated using the expression $(1-b)$[46]. The slow inactivation variable for *Shab*, and the activations of *Shal*, and *Shaker* were assumed to be equal to one[29,47]. The inactivation variables of *Shal* and *Shaker* channels are respectively l

and h. Note that the steady state inactivation variable of *Shal* channels is less than or equal to the inactivation of *Shaker* for any value of v. As a consequence, *Shal* channels have different effects on membrane depolarizations compared to *Shaker* channels. The resulting currrents in the model are:

$$I_{Na} = \bar{a}_{Na} \cdot m_\infty^3(v)(1-b) \cdot sinh[\frac{q}{2kT}(v - v_{Na})] \tag{4.15}$$

$$I_K = I_b + I_h + I_l = (\bar{a}_b b^4 + \bar{a}_h h + \bar{a}_l l) \cdot sinh[\frac{q}{2kT}(v - v_K)] \tag{4.16}$$

$$I_L = \bar{a}_L \cdot sinh[\frac{q}{2kT}(v - v_L)] \tag{4.17}$$

where m, b, h, and l represent, respectively, gating variables for Na^+ channel activation, *Shab* activation, inactivation of *Shaker*, and inactivation of *Shal*. The terms $\bar{a}_{Na}$, $\bar{a}_b$, $\bar{a}_l$, $\bar{a}_h$, and a $\bar{a}_L$ represent, respectively, the maximal whole-membrane amplitudes of the Na^+, delayed rectifier, *Shal* and *Shaker* A-type, and leak currents. These amplitudes can be thought of as multiples of the numbers of channels mediating each current[40,42]. That is, the maximal current amplitudes in the model can be thought of in terms of channel expression.

Biophysical Model of Neuron Membrane Potential

The equation for v can be factored to allow regrouping of the maximum current parameters so that the maximum rate of change of v in the model can be fit to data, and so that the contributions of the different currents are now written as proportions of the different channels relative to the number of Na^+ channels. The resulting system takes the form:

$$\begin{aligned} \dot{v} &= k \cdot [J - J_{Na} - J_K - J_L], \\ \dot{w} &= (w_\infty - w)/\tau_w, \quad w \in \{b, h, l\} \end{aligned} \tag{4.18}$$

The ionic currents are rewritten as

$$J_{Na} = m_\infty^3(v)(1-b) \cdot sinh[\frac{q}{2kT}(v - v_{Na})] \tag{4.19}$$

$$J_K = (a_b b^4 + a_h h + a_l l) \cdot sinh[\frac{q}{2kT}(v - v_K)] \tag{4.20}$$

$$J_L = a_L \cdot sinh[\frac{q}{2kT}(v - v_L)], \tag{4.21}$$

with

$$k = \frac{\bar{a}_{Na}}{C_m}, \quad J = \frac{I}{\bar{a}_{Na}}, \quad a_x = \frac{\bar{a}_x}{\bar{a}_{Na}} \tag{4.22}$$

The constant k can be used to obtain maximum amplitudes of the time-dependent rate of change of membrane potential δ_v/δ_t, comparable to experimentally measured rates of change, usually between 50 and 250 mV/ms[48]. The factorization of a_{Na} in Eq. (4.18) is convenient because it allows an easy adjustment to the rate of change in membrane potential to fit physiological data. The factorization is that simulations and results can be interpreted in terms of the relative presence of channels in the membrane with respect to the Na^+ channel population.

Modeling Different Membrane Channel Expression

Balance rules between the different proportions of channels in the membrane were designed with the idea of grouping parameters and study the influence of changes in channel expression on the excitability of system. This approach could also be used to model possible homeostatic mechanisms in which the relative presence of Na^+ and K^+ channels is conserved to maintain excitability levels[11,38,49,50]. For example, the ratio of K^+ to Na^+ currents

$$r_{KNa} = \frac{a_b + a_h + a_l}{a_{Na}} \tag{4.23}$$

can be set to a constant so that only the ratios of *Shab*, *Shaker*, and *Shal* are systematically changed. To do so, the population of K^+ channels is partitioned into two groups, the persistent and the transient (A-type) channels. A subsequent partition of the population of A-type channels was obtained by considering the quantities

$$r_{bK} = \frac{a_b}{a_b + a_h + a_l}, \tag{4.24}$$

$$r_{hA} = \frac{a_h}{a_h + a_l}, \tag{4.25}$$

which can be thought of as, the proportion of persistent K^+ current relative to the total K^+ current (4.24), and the proportion of *Shaker* current relative to the total A-type current (4.25), respectively. Note that the proportion of A-type current relative to the total K-current is then r_{AK} = 1 - r_{bK}. Similarly, the proportion of *Shal* relative to the total A-current is r_{lA} = 1 - r_{hA}. Assuming no changes in the leak current, the ratios r_{bK} and r_{hA} may be systematically varied to represent different

combinations of K^+ channel populations in the membrane. To do so, the ratio of r_{KN} a is set to a constant, and values for a pair (r_{bK}, r_{hA}) are selected. For example, (r_{bK}, r_{hA}) = (0.9,0.3) represents the case in which nine of every ten K^+ channels are persistent, and for every ten A-type channels, three are *Shaker* and seven are *Shal* type.

The amplitude ratios of the model can then be calculated as follows:

$$a_b = r_{KNa} \cdot r_{bK}, \tag{4.26}$$

$$a_h = r_{KNa} \cdot (1 - r_{bK}) \cdot r_{hA}, \tag{4.27}$$

$$a_l = r_{KNa} \cdot (1 - r_{bK})(1 - r_{hA}), \tag{4.28}$$

Note that the maximal whole-membrane amplitudes $\bar{a}_b$, $\bar{a}_h$, and $\bar{a}_l$, can then be calculated if r_{KNa}, r_{bK}, and r_{hA} are known.

Steady States and Bifurcations

One way to determine the computational properties of a model neuron based on Eqs. (4.19)-(4.21) is to examine the following function of v and its concavity

$$J_\infty = J_{(Na,\infty)} + J_{(K,\infty)} + J_{(L,\infty)} \tag{4.29}$$

where $J_{(Na,\infty)}$, $J_{(K,\infty)}$, $J_{(L,\infty)}$ are the channel currents with gating variables b, h, and l in (14)-(16) replaced by their steady states b_∞, h_∞, and l_∞. J_∞ has shape equivalent to a cubic function of v. Note that the system is at a steady state if the total current (J - J_∞) is zero. The number of fixed points equals the number of zeros in (J - J_∞). Let the injected current J be the bifurcation parameter. If J_∞ is monotonic, the number of fixed points is always one because (J - J_∞) has only one zero for each J. The neuron in this case can be near an AH bifurcation. If J_∞ is not monotonic, (J - J_∞) may have one, two, or three zeros depending on the value of J. The transitions from one to two, or two to three fixed points are saddle-node bifurcations. As a consequence, the monotonicity, or lack thereof, in the curve J_∞ determines whether the neuron functions as an integrator or a resonator.

The minimal current amplitude necessary to trigger a sustained spiking response is called *rheobase*. For neurons near a SN bifurcation, the rheobase is the current for which J_∞ has a local maximum. A quick way to determine the rheobase of a neuron is to plot the total current at steady state using

voltage clamp and determine if, and when, the curve is concave up or concave down. If the curve is monotonic, it may still show a bend that continues toward negative values for increasing v. If the (J - J_∞) curve is not monotonic, it is likely to take positive values for small v and negative values for large v. Such curves can be thought of as having three branches: (J - J_∞) decreases as a function of v along the beginning and ending branches, and increases on the middle branch. As a general rule, fixed points that lie on either the beginning or ending branches ($J = J_\infty$ and $-dJ_\infty/dv < 0$) are stable, and fixed points on the middle branch are unstable ($J = J_\infty$ and $-dJ_\infty/dv > 0$). For this reason, if the J_∞ curve has a cubic shape, the middle branch will be called the unstable branch.

Here, the bifurcation type of neurons assumed to have different expressions of K^+ channels are assessed by calculating the steady state current of the system for different combinations of the ratios (r_{bK}, r_{hA}) with fixed r_{KNa} and fixed a_L.

Single spike trains are modeled as a renewal process, i.e. a stochastic point process. The realizations of this process are sinlge points in time (*Perkel, 1967*). These single points in time are presynaptic neuronal spiking events, such that these realizations result in EPSP in the postsynaptic neuron no larger than 0.1 mV. The renewal process is parameterized by a rate parameter r and a refractory period k measured in milliseconds. The refractory period is a period of time in which the neuron can't fire, i.e. the interspike intervals can't be arbitrarily small. At each time step, the probability of a presynaptic neuronal firing event is $p = r * k/T$, where T is the maximum time course of the renewal process measured in milliseconds. At each time step, assumed to be 1 millisecond, a random number is generated between 0 and 1. If this random number is less than $r * k/T$ then there is a spiking event. To account for k msec refractory period, only keep every kth of such spiking events. Specifically for this modeling effort, synaptic input to each neuron ranged from 5-100 spike trains. The sampling time step δ = 1 msec, with rate parameter set at 40 Hz. The refractory period was assumed to be 2 msec.

The excitatory synaptic input is a time dependent process. Spiking events from the presynaptic neuron are determined by realizations from a renewal process. Let the synaptic current be given by:

$$I_s = \kappa A_{syn}(s) sinh(\frac{qz_x}{2kT}(v - v_s)) \tag{4.30}$$

Table 4.1: Physical Constants and Parameters

Physical constants	Description	Value	Units
T	Absolute temperature	296.15	*Kelvin*
k	Boltzman's constant	$1.38065812*10^{-20}$	*mJ/Kelvin*
q	Elementary charge	$1.60217733*10^{-19}$	*Columbs*
z_{Na}	valence of Na^+ ion	1	-
z_K	valence of K^+ ion	1	-
Parameters			
C_M	Membrane capacitance	0.13	μF
v_{Na}	Reversal potential for Na^+	55	*mV*
v_K	Reversal potential for K^+	-72	*mV*
v_L	Reversal potential for leak current	-75	*mV*
v_m	half-activation potential for Na^+	-32	*mV*
v_b	half-activation potential for K^+	-40	*mV*
z_m	Gating charge for Na^+ channel	1.65	*Columbs*
z_b	Gating charge for K^+ channel	1.8	*Columbs*
a_{Na}	maximum Na^+ whole-cell current	16	*nA*
a_K	maximum K^+ whole-cell current	80	*nA*
a_L	maximum leak whole-cell current	4.5	*nA*
I	external source of current	[0,2]	*nA*

κ is an expected value of the number of recruited synapses that equals p times κ. The number of synaptic contacts from one axon collateral of the presynaptic neuron is many, i.e. the single axon process branches into many processes (*Boron, 2003*; Kandel, 1985). The probability of activating one of these many processes is given by p and K is the number of branching processes from the axon collateral, so that κ is an expected value.

The Nernst equilibrium, v_s for excitatory synaptic input is assumed to be zero. The term $A_{syn}(s)$ is the current amplitude of excitatory synaptic input measured in nA. It is given by an alpha function:

$$A_{syn}(s) \quad = \quad an\frac{s}{\tau_n}exp(1-(\frac{s}{\tau_n}))H(s) \tag{4.31}$$

s is the time of activated synapse, determined by the renewal process. The peak synaptic current amplitude is an. Time to peak is given by τ_n. $H(s)$ is a heavyside function (equal to 1 if s>0 and 0

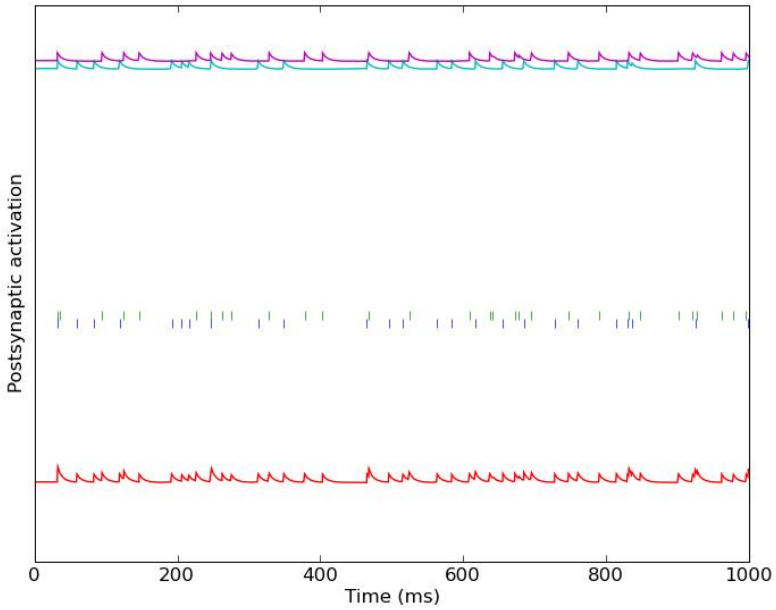

Figure 4.2: Sample of Input Spike Trains Forming a Composite Excitatory Postsynaptic Potential

otherwise). If there is a spiking event at time t_0, there will be a conduction delay δ_{syn} of 0.58 msec. Therefore, the current amplitude of a synaptic event at time t is $A_{syn}(t\text{-}t_0\text{-}\delta_{syn})$.

The synaptic input is considered to be excitatory. A synaptic event of the presynaptic neuron will depolarize the membrane of the postsynaptic neuron, i.e. the synaptic event triggers an EPSP. The membrane depolarization from a single synaptic event results in an EPSP of 0.1 mV. It generally takes many EPSPs to generate an action potential from the postsynaptic neuron.

4.3 Integrator and Resonator Dynamics

In dynamical systems terms, neurons are excitable because the resting membrane potential is near a bifurcation. The spike-intiating mechanism or the transition from resting to spiking confers specific neuro-compuatational properties. The spike-initiating mechanism is uniquely determined by the bifurcation structure. In the seminal report by Rinzel and Ermentrout, they summarize that general models of the form above display qualitatively different threshold behavior when the steady state current-voltage relation is monotonic or non-monotonic (*Rinzel & Ermentrout, 1989*). The response properties from integrators are qualitatively and quantitatively different than resonators. Fig. 4.5

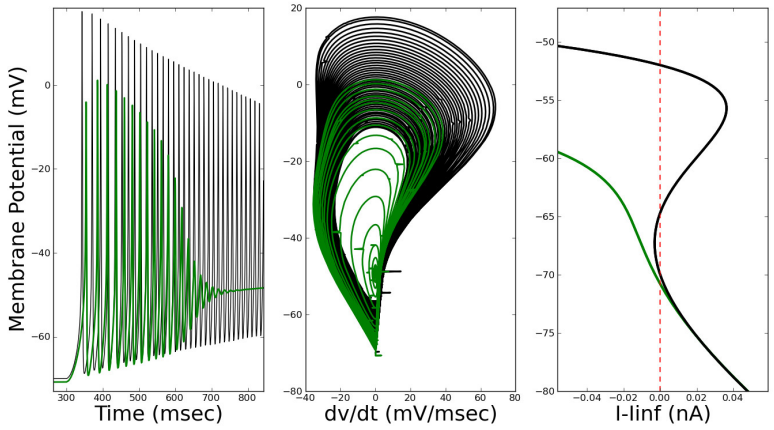

Figure 4.3: Integrator and Resonator Dynamics

displays the integrator's spiking output to excitatory spike trains. The spike trains increase from 1 to 200. As the number of spike trains increase, the firing frequency of the integrator increases. Hence, the relationship between the number of excitatory synaptic input and firing frequency is monotonic.

Fig. 4.4 displays the spiking output of the resonator to excitatory spike trains. Here we notice a fundamental difference in response properties as compared to integrators as in Fig. 4.5. The resonator firing frequency at first increases and then decreases to excitatory synaptic input, therefore the relationship is non-monotonic.

These preliminary findings confirm the hypothesis that integrators and resonators respond differently to excitatory synaptic input. These results illustrate the importance of modeling the nonlinear dynamics of neural memebrane potential. Neurons that merely integrate synptic input is only capturing part of the story. As fundamental units of information processing, neurons transform and process synaptic input in qualitatively different ways.

4.4 Analysis of Spike Trains

The following section outlines the methods used to quatify the spike trains. Beginning with descriptions and definitions of spiking rates, interspike intervals, the section then describes ways to quantify correlated spiking among two neurons. This includes correlation functions and their associated measures. In order to assess significant flucuations in the correlation functions, the correction

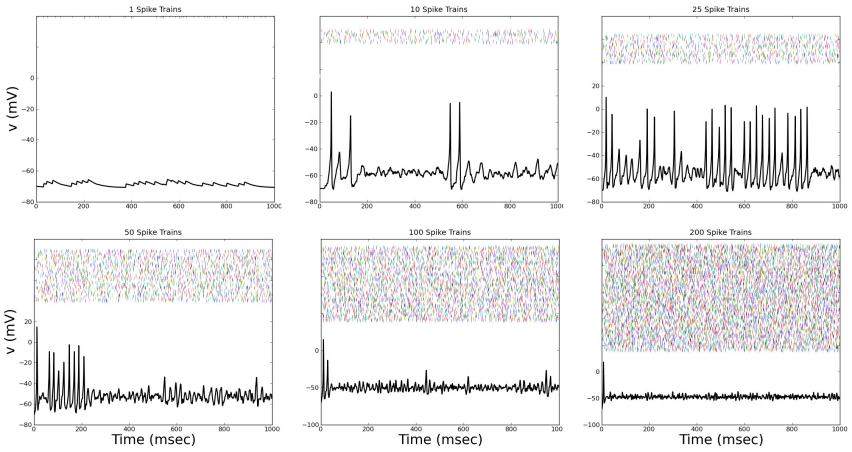

Figure 4.4: Resonator Neuron Driven by Excitatory Synaptic Input

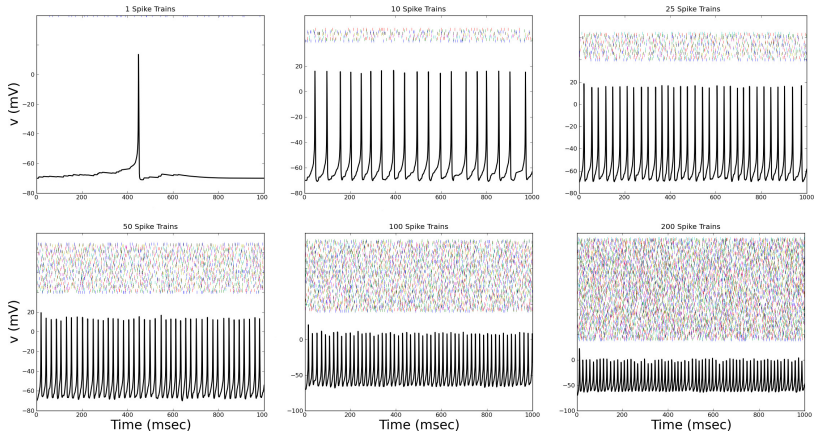

Figure 4.5: Integrator Neuron Driven by Excitatory Synaptic Input

for independence method is described and implemented. Finally, the last section describes two indices of spiking synchronization, namely *k* and *CIS*.

Spike Trains: Definitions and Basic Quantification

Assume the membrane potential is a function of time with time steps of δ_t in the interval $[0,T]$. Also, assume also time is in units of milliseconds (*ms*). By setting a threshold value for the membrane potential, a spike time can be defined as the time when the membrane potential passes such threshold. A spike train is then defined as a sequence of spike times.

Counting Spikes Using Pulsed Functions. It is convenient to describe spike trains by means of

time-dependent delta-functions defined as

$$\delta(t) \quad = \quad 1 if t = 0, 0 otherwise \tag{4.32}$$

Using the delta function in combination with the spike times, the spike train can be written as a function of time

$$s_t \quad = \quad \sum_{i=1}^{N} \delta(t - t_i) \tag{4.33}$$

The notation used in Eq. (3.2) is very useful because it provides with a framework for quantification of spike trains. For example, it is now possible to write a formula for the number of spikes in the train within a time interval [a,b]:

$$C([a,b]) \quad = \quad \sum_{t \in [a,b]}^{N} s_t \tag{4.34}$$

The probability of observing a spike in the interval [a,b] can be approximated by dividing the spike count from Eq. (3.3) by the length of the time interval:

$$R([a,b]) \quad = \quad \frac{C([a,b])}{b-a} \tag{4.35}$$

Notice that to obtain R in units of pulses per second (pps) it would be necessary to multiply by 1000.

A spike train is called *stationary* if the probability of finding a spike in an interval of length T is the same regardless of the location in the recording and of the size of the interval T. In other words, the train is *stationary* if the neuron from which the train was recorded can be expected to fire, on average, the same number of action potentials within any two time-intervals of the same length. A consequence of stationarity is that if N is the average number of spikes in T *ms*, then $R(0,T)$ = N/T will converge to the true probability of spiking as T increases. Consequently, if a spike train is stationary, the count in (3.3) only depends on the length of the interval and $R(0,T)$ can be regarded as the average spike frequency in an interval of length T, provided T is long enough(see Fig. 3.2).

Now let τ be a random variable representing the waiting times between spikes, or *interspike intervals* from a spike train. Then, for the spike train t_0,..., t_N, τ takes values $\tau_i = t_i$ - t_{i-1} for i = 1,..., N. A count of the interspike intervals can be calculated using delta functions:

$$D(t) \quad = \quad \sum_{i=1}^{N} \delta\{\tau_i = \tau\} \tag{4.36}$$

A plot of D for each value of τ is the histogram of interspike intervals. The variability of interspike intervals is usually assessed by calculating the *coefficient of variation* of the interspike intervals, $_\tau$, defined as the quotient between the mean and the standard deviation of the interspike intervals, $s_\tau/\bar{\tau}$.

The multiplicative inverses of the interspike intervals form a sequence $f_1 = 1/\tau_1$,..., $f_N = 1/\tau_N$ called the *instantaneous firing rates*. To express the rates in units of pulses per second (pps), the instantaneous firing rate of the train can be obtained by multiplying each of the elements of the sequence f_1,..., f_N by 1000.

The *average firing frequency* of the neuron can be approximated by calculating the multiplicative inverse of the average interspike interval, $1/\bar{\tau}$. It can be demonstrated assuming that spike trains are stochastic point processes that the inverse of the average interspike interval $1/\bar{\tau}$ converges to the true spiking rate for large enough T. Another approximation that is accurate only in a limited number of cases can be obtained by calculating the average of the instantaneous firing rates, $\bar{f}$.

Quantification of Joint Spiking Activity

Let two spike trains be represented by the sequences $q_i^{(1)}$ and $q_j^{(2)}$, where $i = 1,..., N_1$ and $j = 1,..., N_2$. Assume train 1 has less than or equal spikes than train 2. Train 1 will be referred to as the reference train and train 2 will be referred to as the response train. Following the notation introduced above, let the spike trains from two different neurons be represented by pulse functions, this time indexed $s_1(t)$ and $s_2(t)$ for $n = 1, 2$. One way to assess if the two spike trains s_1 and s_2 are independent is to calculate their correlation function. In a continuous setting, correlation functions are just convolutions of two time dependent functions. In a discrete space like the time sample described here, the correlation function between two spike trains is written as

$$C_{2,1}(h)$$

where h is a time difference or delay between a spike in the response train and a spike in the reference train. The values for h are typically chosen to be within a relevant time scale for the phenomenon under study. For example, in situations where synchronous spiking is studied, the typical interval for h is [-100, 100] *ms*. The count is then repeated for different values of h, thus obtaining a function that depends on the time-delays between spikes from the two trains. This function is often called *cross-correlation* function if the two trains are different and *auto-correlation* function if the

same train is used as response and as reference. Note that $C_{1,2}(h) = C_{2,1}(-h)$, so it is not necessary to do another calculation to obtain $C_{2,1}(h)$.

The correlation function (3.6) counts the number of spikes from neuron 2 that occur h units of time apart from a spike from neuron 1. In other words, the function $C_{1,2}$ counts the number of *joint spikes* between neurons 1 and 2 at different time delays (Fig. 1.1 and 3.3). The graph of a correlation function (3.6) as a function of the time-delay h is called is a *correlogram*. Such a graph is often called *cross-correlogram* if the two spike trains are different. Similarly, if the reference and response trains are the same then the graph is also called *auto-correlogram*.

Chapter 5

BIOPHYSICAL MECHANISM FOR NEURAL SPIKING DYNAMICS

5.1 Spiking Dynamics of Neurons with Realistic Excitatory Synaptic Input

In honey bee studies, uPNs initially fire at rates within the 30-45 Hz range in response to constant odor stimulation (*Nawrot, 2010*). The number of inpt axons N_a was determined to be between 300–400 in order that the uPNs spike at a rate between 30–45 Hz. Here, the ORNs which form the presynaptic input each fire at a rate of 25 Hz.

Once the simulations have the uPNs firing within physiological rates, the coefficient of variation

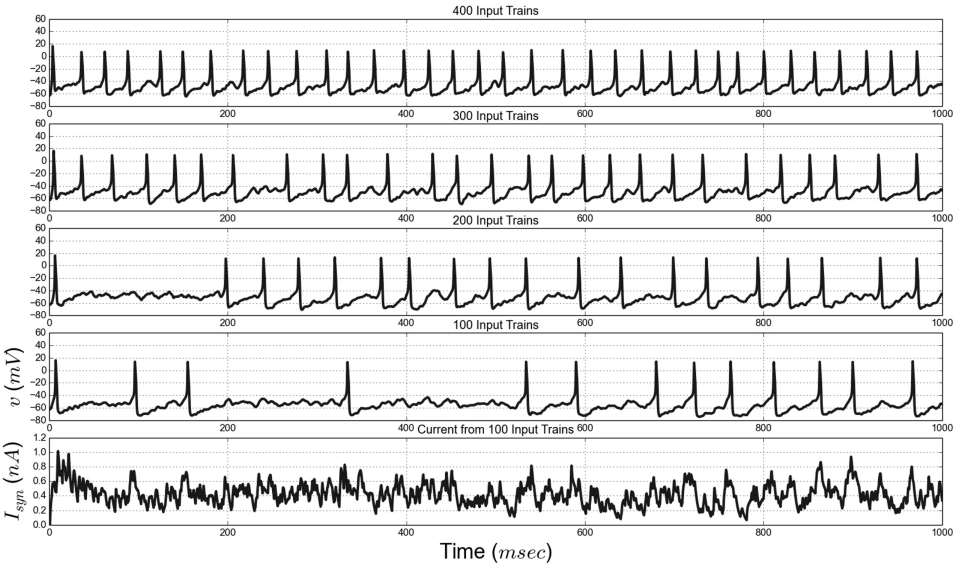

Figure 5.1: Spiking Dynamics of Projection Neurons to Increasing Number of Input Trains

CV_{isi} was calculated of the uPN interspike intervals ranging between 0.2 and 0.42. The simulations were implemented with p_s (the probability of synaptic activation) within the following ranges: [0-0.85]. Keeping all other parameters constant resulted in larger EPSPs with larger values of p_s.

As shown in Fig. 5.1, increasing the number of ORN axon collaterals from 100 to 400 results in a uPN to increase its firing rate. The bottom panel in the previously mentioned figure shows an example of the total presynaptic current from 100 ORN axons as an illustrative example.

The results from 200 simulations with the proportion of common presynaptic input increasing

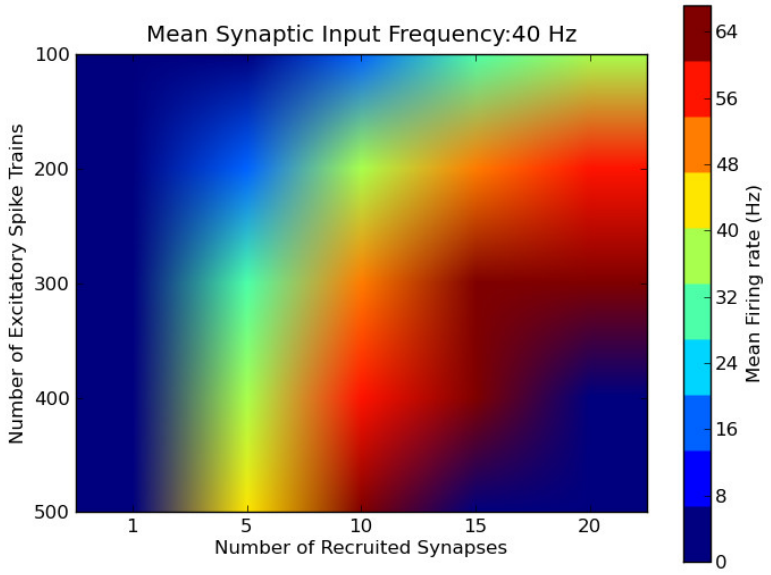

Figure 5.2: Spiking Dynamics of Projection Neuron Near Andronov-Hopf Bifurcation

from 0 to 1. Here, the duration of each trial input condition was help constant, i.e., $P(CEI)$ was held constant for a total simulation time of 100 seconds. In order to detect the central peaks, the previously described method is implemented to delimit the central peak. Recall, the theoretical prediction for the number of joint spikes that occur given both neurons are independent is used to delimit the central peak. If $P(CEI) < 0.1$ there was no significant flucuation around time-delay zero, i.e., the central peak could not be detected. Furthermore, a central peak could be detected if $P(CEI) > 0.1$ and becomes more prominent as $P(CEI)$ approaches 1.

Differential Contribution of Potassium Currents to Neuronal Excitability

The current section includes model simulations and predictions obtained from the system of Eqs. (4.18)-(4.22) with different combinations of K^+ channels. The predictions made in the current section are then discussed in consideration of data from experiments focusing on knock-out/down of K^+ channel genes. Possible applications of the model are also discussed, followed by a general commentary about biophysical modeling, protein expression and physiology.

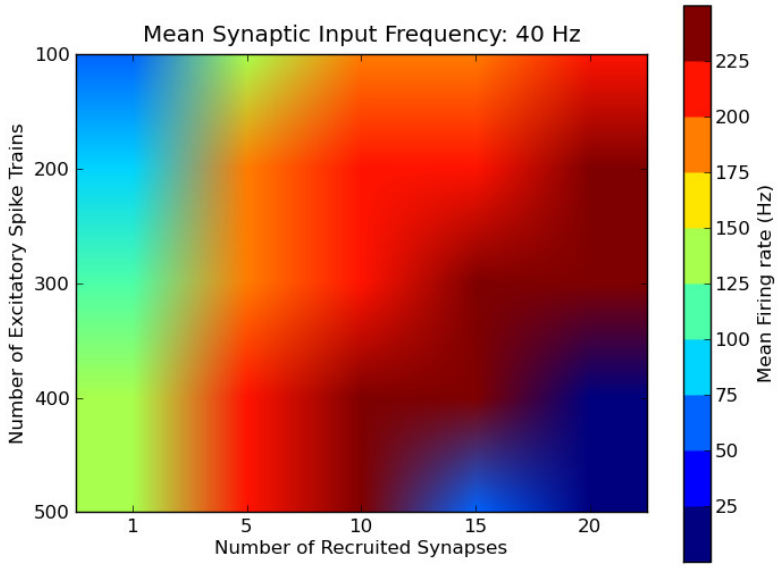

Figure 5.3: Spiking Dynamics of Neuron Near Saddle-Node Bifurcation

Membrane excitability without A-type K^+ channels. The gating parameters for the Na^+ and K^+ channels cause this model with only two currents to display resonator characteristics. That is, if the stimulus amplitude is large enough, the transition from rest to spiking occurs through a AH bifurcation. Both the data and the model display a delay to first spike that decreases with stimulus amplitude. Initially, with low stimulus amplitudes, no spiking responses are triggered (not shown). Then, if the stimulus is large enough, a single spike may be triggered, followed by a dampened oscillation. Repetitive spiking emerges as stimulus amplitude increases, and it is eventually replaced by a dampened oscillation around a new resting value that depends on the stimulus amplitude. These three different regimes, i.e. depolarization without spiking or with possibly only one spike after some delay, repetitive spiking, and depolarization possibly including a single spike followed by a dampened oscillation, have been described in uPNs and in other neurons as outlined above. These three different kinds of response are generalizations of classifications of experimental data proposed previously (see [3] and [5]). The first and last cases in which the membrane potential tends toward a specific level (either the resting potential or a depolarized potential) correspond to cases in which

the model neuron has a stable fixed point and it is near an AH bifurcation. In the first case the neuron is excitable; in the later case the neuron is block-depolarized. The case in which repetitive spiking occurs is one in which the model neuron has an unstable fixed point, and the membrane evolves toward a limit cycle attractor. Repetitive spiking occurs because the increase in injected current causes the system to undergo a bifurcation of the steady state in which an attracting fixed point becomes unstable as it gives rise to a limit cycle (rest to spiking) that increases in amplitude, and eventually shrinks to a small amplitude oscillation in which v eventually converges to some depolarized value. If the stimulus is further increased, the system undergoes another AH bifurcation, in which the fixed point becomes stable again.

To explore additional properties that A-type K^+ channels may confer to a neuron, we add the two voltage-dependent, A-type K^+ channels *Shal* and *Shaker* to the model. To do so, we assume that the total contributions of both the leak and the K^+ currents are constant relative to the contribution of the Na^+ channels. As described in the Methods section, these assumptions allow systematic study of the differential contribution of K^+ channels in the model to the membrane dynamics. Then only *Shal*, only *Shaker*, and both *Shaker* and *Shal* are included among the K^+ channels in the model. The different properties displayed in the presence and absence of A-type channels are discussed in terms of bifurcations of the steady state.

Contribution of Shal channels to membrane excitability. Simulations in which only *Shal*, and no *Shaker* A-type K^+ channels are added to the reference model are shown. Recall that *Shal* channels are the first to inactivate. The thick gray lines illustrate, for reference, the responses obtained with the two dimensional model without A-type channels. The black and blue lines correspond to models in which more *Shal* channels were subsequently added to the membrane. The ratios and parameters used for for these simulations were $r_{KNa} = 5$, $r_{bK} \in \{1, 0.8, 0.6\}$, and $r_{hA} = 0$. Panels A-C show simulations of different voltage responses corresponding, respectively, to stimulus amplitudes of 0.25, 0.5, and 0.75 nA . The insets show the voltage traces around the stimulus time ($t_{stim} = 50$ $msecs$). The responses in all traces show how that the delay to first spike is shorter as the stimulus increases, but the delay to first spike is always more prominent with more *Shal* channels. Importantly, the spike frequency becomes very similar to that of the model with no A-type channels as the stimulus amplitude increases.

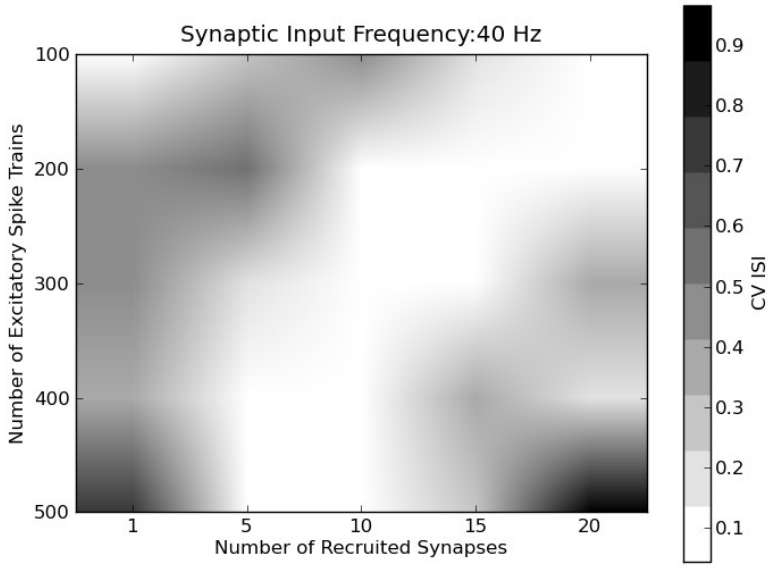

Figure 5.4: Coefficient of Variation of Spiking Rate of Neuron with Resonator Dynamics

A and B show examples in which the stimulus amplitudes are large enough to trigger repetitive spiking responses. Importantly, the spiking frequency is faster than the frequency in the model with no A-type channels. The stimulus amplitude may be large enough to push the system beyond the the repetitive spiking regime. This happens when the fixed point of the system associated with the resting potential is not the same before and during the stimulation, but in both cases it is stable. In this case, the stimulus bypasses the regime in which the neuron displays repetitive spiking as shown in panel C.

The total steady state current I - I_∞ (gray, black and blue curves) is shown for different stimulation levels (vertical lines). The fixed points of the system in panels A, B, and C are at the crossing between the vertical lines indicating the input current and the I - I_∞ curves. As pointed out previously, the reference curve (thick gray) from the model without A-type channels is monotonic, indicating that in this case, the model neuron is a resonator with resting state near an AH bifurcation. As a consequence, there is only one zero crossing for I - I_∞ for the reference model, illustrating that the transition to repetitive spiking is not manifested as a change in the number of fixed points,

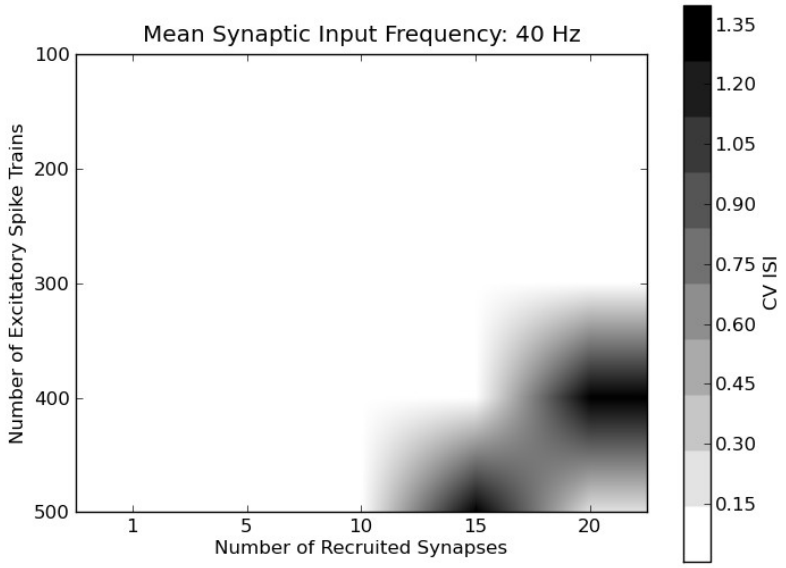

Figure 5.5: Coefficient of Variation of Spiking Rate of Neuron with Integrator Dynamics

but only as a change in the stability of the fixed point.

Adding more *Shal* channels causes the I - I_∞ curve to lose its monotonicity, causing the transition between rest and spiking states to occur via a SN bifurcation. For illustration purposes, think of the line at $I = 0$ moving slowly toward the left. At first, the intersection of the vertical line with any of the curves would be only one point, but as the line continues to move to the left, there are be two, three, two and then one intersection points for the blue and black curves, indicating that the system undergoes a SN bifurcation of the steady state as current injection increases. Taken together, these simulations support the hypotheses advanced by Choi et al. and others[3,25] implicating the *Shal* channels as responsible for the delay to spiking in neurons. In terms of the computational properties of the cell, *Shal* channels confer integration capabilities to neurons by changing the bifurcation structure in such a way that the steady state bifurcates via a SN bifurcation[1].

Contribution of Shaker channels to membrane excitability. To investigate the contribution of Shaker channels to the membrane excitability, the proportions of K^+ channels are changed so that only *Shab* and *Shaker*, but no *Shal* channels are present in the membrane, again, maintaining a

constant maximum whole-membrane K^+ current. hows simulated voltage responses for a procedure similar to that used in the case of Shal, with the thick gray curve showing the reference model without A-type currents, and the black and blue curves illustrating cases with increasing amounts of *Shaker* channels. In this case, the proportion of *Shal* channels a_l is set to zero, and increasing amounts of *Shaker* channels are considered corresponding to $r_{AK} \in \{0, 0.1, 0.3\}$. As before, A-C show voltage traces corresponding to different current stimulus amplitudes, and panel D illustrates the bifurcation structure of the model when the only K^+ channels are *Shab* and *Shaker* type. Importantly, the A-type current relative to all K^+ current for *Shaker* only was to be very small in comparison to the case when only *Shal* channels were present ($r_{bK} \in \{0.997, 0.9975, 1\}$). Recall that inactivation of Shaker channels is incomplete for membrane potentials close to rest and the likelihood that *Shaker* channels are open is larger than that of *Shal* channels as a function of v. The hypothesis that Shaker channels have a larger, dampening effect on membrane excitability was tested, and confirmed by adding a very small fraction of *Shaker* channels, which resulted in no spiking for current stimulation up to about 0.25 nA. As the stimulus amplitude increases, the neuron eventually exhibits single spikes, and in some cases, repetitive spiking, if the stimulus amplitude is large enough.

The delay to first spike exhibited previously is still present but to a lesser extent. Importantly, the bifurcation structure does not change type; in this case, the I - I_∞ curves do not loose their monotonicity, indicating that the neurons never switch from resonator to integrator, in contrast to the results obtained when adding only Shal channels.

Chapter 6

SUMMARY AND CONCLUSIONS

6.1 Summary

I have provided theoretical arguments supporting previously advanced hypotheses about the differential contribution of A-type voltage-gated K^+ channels to the behavior of neuronal membranes. To do so, a biophysical model of membrane potential is used, which provides with a controlled setting where every factor influencing the membrane dynamics is known. This way, factors like the nutrient concentration in bath solutions, light, temperature, etcetera do not influence the results. Interpretations can thus be made solely in terms of voltage-dependent properties and relative numbers of the channels in the membrane. This approach requires macroscopic parameters describing channel kinetics and whole membrane currents. These choices allowed us to be consistent in our formulations. Biophysical formulation of membrane potential also capture behaviors displayed by other Drosophila neurons (other adult, larva or embryonic motor neurons, or even giant cultured neurons or some Kenyon cells). This can be accomplished by choosing different proportions of channels in the membrane (not shown).

The types of A-channels were restricted to only include *Shal* and *Shaker* for the following reasons. First, the reported voltage dependencies of Drosophila A-type channels Shal, Shaker, and Slo can be classified into two groups defined by their voltage-dependent inactivation. The two groups are formed, respectively, by Shal, and by Shaker. Second, the voltage-dependence of calcium dependent A-type channels, overlaps with the voltage- dependence of Shaker. For these reasons, the results presented are only in terms of *Shaker* and *Shal* are adequate to generally describe the role of A-type channels in shaping rest to spiking transitions.

Choi et al and many others have hypothesized that expression of the A-type K^+ channel gene Shal (analog of the vertebrate Kv_4) is responsible for delayed spiking responses in different kinds of Drosophila neurons (*Choi, 2004*). Choi et al. characterized the electrophysiological activity of Drosophila larval motor neurons in recordings made using voltage and current clamps in combination with pharmacological and genetic manipulations (*Choi, 2004*). Choi et al. described qualitative and quantitative differences in the delay to first spike in response to square pulses of stimulation.

After different experiments that included recordings from Shaker mutant neurons and pharmacological manipulations, Choi et al. demonstrated that spike delay is sensitive to prepulse-sensitive K^+ currents. Further, they showed that Shaker channels do not play a significant role in determining delay to the first spike or the spike rate in Drosophila larval neurons. As a consequence, Choi and his coworkers postulated the hypothesis that Shal channels, not Shaker, are responsible for the delay to first spike under square pulse stimulation. Saito and Wu had similar hypotheses but their studies did not focus specifically on this issue (*Satio & Wu, 1991*). The role of Shal channels in producing spiking delays in response to excitatory input was adressed only indirectly because Shal mutants or RNA-interference (RNAi) lines were not available. Importantly, a consequence is that Shaker and Shal channels (or their analogs from the Kv_1 and Kv_4 respectively) confer different computational properties to neurons. More specifically, these two channels allow neurons to switch between integration and resonation modes (respectively, depolarization only- vs input-frequency induced spiking).

I have shown that different qualitative behaviors experimentally observed in a variety of Drosophila neurons can be reproduced for a minimal complement of currents (fast Na^+ and delayed rectifier K^+) with fixed gating kinetics, and where the only free parameter allowed was the ratio between K^+ and Na^+ channels. The voltage traces illustrate the sequence of behaviors one should expect for responses to current injection. Roughly speaking, for small enough current amplitudes, the membrane depolarizes but tends toward a higher membrane potential without any spiking (no change in the stability of the fixed point of the system). Large enough stimulus amplitudes should cause the membrane to loose its stability and transition into a repetitive spiking mode, and if the stimulus is large enough, depolarization block should occur. Experimentally, the window for which the stimulus amplitude causes repetitive spiking may be very small, which explains why some neurons never show repetitive spiking but spike once for large enough amplitudes.

Without A-type channels the neuron has a monotonic I - I_∞ curve, which indicates that the membrane may exhibit post-inhibitory rebound and resonant repetitive spiking with an interval of input frequencies. In other words, the Shab-Na neuron is a resonator for a wide range of ratios between K and Na channels (not shown). To address the differential contribution of the voltage-dependent A-type K^+ channels Shal and Shaker, a computational knock in experiment was performed in which

either Shal, Shaker, or both channels were inserted in the membrane in different proportions. Recall that these two channels differ mainly in their voltage-dependent inactivation. Note the approach taken here is incremental in the sense that channels are added one at a time to a simpler membrane. In contrast, experimental protocols usually involve pharmacological or genetic targeting of single channels with the intention of functionally blocking, knocking-out, or knocking-down specific proteins of interest.

The presence of A-type channels has the following general effects on the membrane dynamics: first, the rheobase increased as the contribution from the A-type channels increased. Also, the firing frequency decreased as more A-type channels were present in the membrane. Similar increases in frequency were reported by Choi et al. for larval motor neurons, by Tierney and Harris-Warrick for different cell types in the pyloric circuit, and theoretically using a generic Hodgkin-Huxley model by Neher, Connor et al., and others (*Neher, 1971*;*Connor et al, 1977*; *choi, 2004*). Our simulations agree with previous modeling results predicting that, in general, A-type channels change the shape I - I_∞ curve from monotonic to N-shaped (*Rush, 1995*). However, I also found that In addtion, I found that rest-spiking transitions in the cell change in qualitatively different ways depending on the relative presence of the different A-type channels. More specifically, increasing numbers of A-type channels with higher half inactivation potentials (Shaker, Kv_1) exert a weak effect on the shape of the I - I_∞ curve such that the change in the I - I_∞ curve may not be noticeable at first. That is, membranes with Shaker and Shal can have non-monotonic I - I_∞ relationships and display long delays to first spike, and further, the long component delay to first spike is caused by Shal.

Insertion of Shal channels into the Shab-Na membrane without Shaker changed the shape of the I - I_∞ curve to non-monotonic, indicating that the membrane at rest was moved closer to a SN bifurcation. In this case, the membrane can be thought of as an integrator of input, and would normally not show post- inhibitory rebounds or resonator properties. Delays to first spike in response to square pulses of current injection increased with the number of Shal channels in the membrane. These results are in agreement with the hypothesis that Shal channels underlie the delay to first spike observed in many Drosophila neurons, including giant cultured neurons, larvae and adult motor neurons, as well as neurons from Tritonia, Aplysia, and lobster (*Tsunoda, 1995*).

In contrast, the monotonicity of the I - I_∞ curve remained unchanged for a wide range of Shaker

channel densities in the absence of Shal. However, larger proportions of Shaker channels result in non-monotonic I - I_∞. The traces in illustrate that the delays to first spike in response to square pulses of current injection are shorter (less than 5 milliseconds). These shorter delays decreased further as the amplitude of the pulses increased. More exhaustive analysis of the monotonicity of I - I_∞ suggests that larger proportions of Shaker are needed to push the membrane away from the resonator regime in comparison to Shal. Taken together, the results from our knock-in simulations suggest that A-type channels can confer different computational properties to a cell as a function of their voltage-dependent inactivation.

To summarize, I have presented sound theoretical arguments supporting the hypothesis that *Shal* channels underlie the delay to first spike displayed by many types of neurons in insect systems. The model is based on insect data of channel kinetics, whole membrane currents, and whole cell behavior. These results can be interpreted as a consequence of cellular biophysics without external influences such as modulation, bath application, etc. The model highlights the theoretical strength of the results obtained experimentally by Choi et al. and others (*Choi, 2004*). Taken together, the simulations shown here for the case of honey bee in combination with the current knowledge about A-type channels, indicate that *Shal* (Kv_4), can be theoretically regarded as mediating excitation delay mechanisms in cells. Moreover, the mixture of different K^+ channels potentially allows cells to operate in different modes, namely, integrating or resonating with synaptic input. The results presented here were produced using a reduced complement of channels and explain a number or experimental observations from neurons which certainly have many more channels. These observations highlight the fact that the wide variety of ion channels expressed in a cell confers different degrees of specialization and contributes to very specific cellular functions, but only a few different channels will are necessary to determine the cells excitability profile.

BIBLIOGRAPHY

1. Abel, R., Rybak, J., and Menzel, R. (2001). Structure and response patterns of olfactory interneurons in the honeybee, Apis mellifera. J. Comp. Neurol. 437, 363383.

2. Choi, J., Park, D., Griffith, L. (2004). Electrophysiological and morphological characterization of identified motor neurons in the Drosophila third instar larva central nervous system. Journal of neurophysiology 91: 2353.

3. Connor, J., Stevens, C. (1971). Prediction of repetitive firing behaviour from voltage clamp data on an isolated neurone soma. The Journal of Physiology 213: 3153.

4. Connor, J., Walter, D., McKown, R. (1977). Neural repetitive firing: modifications of the Hodgkin-Huxley axon suggested by experimental results from crustacean axons. Biophysical Journal 18: 81102.

5. Denker M, Finke R, Schaupp F, Grn S, Menzel R (2010) Neuronal correlates of odor learning in the honeybee antennal lobe. Europ J Neurosci 31: 119-133.

6. Duch, C., Vonhoff, F. & Ryglewski, S. (2008). Dendrite elongation and dendritic branching are affected separately by different forms of intrinsic motoneuron excitability. Journal of Neurophysiology 100: 2525.

7. Ellaway, P.H. Cumulative sum technique and its application to the analysis of peristimuls time histograms. Electroencephalogr. Clin. Neu- rophysiol., 45:302304, 1978.

8. Esslen, J., and Kaissling, K. E. (1976). Number and distribution of sensilla on antennal flagellum of honeybee (Apis mellifera L). Zoomorphologie 83, 227251.

9. Eugene Izhikevich. Dynamical Systems in Neuroscience. MIT, MIT Press, 55 Hayward Street, Cambridge MA 02142, 2007.

10. Eugene M. Izhikevich. Simple model of spiking neurons. IEEE Trans- actions on Neural Networks, 14(6):15691572, 2003.

11. Evyatar Av-Ron, Hanna Parnas, and Lee A. Segel. A basic biophysical model for bursting neurons. Biological Cybernetics, 69:8795, 1993.

12. Faber T, Joerges J, and Menzel R (1999) Associative learning modifies neural representations of odors in the insect brain. nature neuroscience 2:74-78.

13. Farooqui, T., Robinson, K., Vaessin, H., and Smith, B. H. (2003). Modulation of early olfactory processing by an octopaminergic reinforcement pathway in the honeybee. J. Neurosci. 23, 53705380.

14. Fernandez, P. C., Locatelli, F. F., Person- Rennell, N., Deleo, G., and Smith, B. H. (2009). Associative condi- tioning tunes transient dynamics of early olfactory processing. J. Neurosci. 29, 1019110202.

15. Farooqui T. (2007). Octopamine-mediated neuromodulation of insect senses. Neurochem Res. 2007;32:15111529.

16. Farooqui, T. (2012). Review of octopamine in insect nervous systems. Open Access Insect Physiology, 4, 1-17.

17. FitzHugh, R. (1961). Impulses and physiological states in theoretical models of nerve membrane. Biophysical Journal, 1:445466.

18. Fonta, C., Sun, X. J., and Masson, C. (1993). Morphology and spatial- distribution of bee antennal lobe interneurons responsive to odors. Chem. Senses 18, 101119.

19. Galizia, C. G., McIlwrath, S. L., and Menzel, R. (1999). A digital three-dimensional atlas of the honeybee antennal lobe based on optical sections acquired by confocal microscopy. Cell Tissue Res. 295, 383394.

20. Galizia, C. G., and Rssler, W. (2010). Parallel olfactory systems in insects: anatomy and function. Annu. Rev. Entomol. 55, 399420.

21. Galizia, C. G., and Sachse, S. (2010). Odor coding in insects, in The Neurobiology of Olfaction, ed A. Menini (Boca Raton, FL: CRC Press), 3567.

22. Girardin, C. C., Kreissl, S., and Galizia, C. G. (2013). Inhibitory connections in the honeybee antennal lobe are spatially patchy. J. Neurophysiol. 109, 332343.

23. Grohmann, L., Blenau, W., Erber, J., Ebert, P. R., Strnker, T., and Baumann, A. (2003). Molecular and functional characterization of an octopamine receptor from honeybee (Apis mellifera) brain. Journal of neurochemistry, 86(3), 725-735.

24. Grnbaum, L., and Mller, U. (1998). Induction of a specific olfactory memory leads to a long-lasting activation of protein kinase C in the antennal lobe of the honeybee. The Journal of neuroscience, 18(11), 4384-4392.

25. Grnewald, B., and Wersing, A. (2008). An ionotropic GABA receptor in cultured mushroom body Kenyon cells of the honeybee and its modulation by intracellular calcium. Journal of Comparative Physiology A: Neuroethology, Sensory, Neural, and Behavioral Physiology, 194(4), 329-340.

26. Hammer, M. (1993). An Identified neuron mediates the unconditioned stimulus in associative olfactory learning in honeybees. Nature 366, 5963.

27. Hammer, M., and Menzel, R. (1995). Learning and memory in the honeybee. The Journal of neuroscience, 15(3), 1617-1630.

28. Hammer, M., and Menzel, R. (1998). Multiple sites of associative odor learning as revealed by local brain microinjections of octopamine in honeybees. Learn. Mem. 5, 146156.

29. Han K.-A., Millar N. S., and Davis R. L. (1998) A novel octopamine receptor with preferential expression in Drosophila mushroom bodies. Neuron 18, 3650 3658.

30. Heeger, D. (2000). Spike trains and renewal processes. URL www.cns. nyu.edu/ david/handouts/poisson.pdf.

31. Hille, B. (2001). Ion Channels of Excitable Membranes. Sinauer Associates, Inc.

32. Hodgkin, A.L. and Huxley, A.F. (1952). A quantitative description of membrane current and its application to conduction and excitation in nerve. J. Physiol., 117:500544.

33. Hummel, T., and Zipursky, S. L. (2004). Afferent induction of olfactory glomeruli requires N-cadherin. Neuron 42, 7788.

34. Kandel, E., Schwartz, J., and Jessell, T. (2000). Principles of Neuroscience. McGraw-Hill.

35. Kirkwood, P.A. On the use and interpretation of cross-correlation mea- surements in the mammalian central nervous system. J. Neuroscience Methods, 1:107132, 1979.

36. Kirkwood, P.A. and Sears, T.A. The synaptic connections to intercostal motoneurones as revealed by their average common excitatory potential. J. Physiol., 275:103134, 1978.

37. Kirschner, S., Kleineidam, C. J., Zube, C., Rybak, J., Grunewald, B., and Rssler, W. (2006). Dual olfac- tory pathway in the honeybee, Apis mellifera. J. Comp. Neurol. 499, 933952.

38. Kirschner, S., Kleineidam, C., Zube, C., Rybak, J., Grnewald, B., and Roessler, W. (2006). Dual olfactory pathway in the honeybee, Apis mellifera. Journal of Computational Neurology. 499, 933952.

39. Kreissl, S., Eichmller, S., Bicker, G., Rapus, J., and Eckert, M. (2004). Octopaminelike immunoreactivity in the brain and subesophageal ganglion of the honeybee. The Journal of comparative neurology, 348(4), 583-595.

40. Krofczik S, Menzel R and Nawrot MP (2008) Rapid odor processing in the honeybee antennal lobe network. Frontiers in Computational Neuroscience 2:9.

41. Kuhn, A., Aersten, A., and Rotter, S. (2004). Neuronal integration of synaptic input in the fluctuation-driven regime. J. Neuroscience, 24(10):23452356.

42. Laissue, P. P., and Vosshall, L. B. (2008). The olfactory sensory map in Drosophila. Adv. Exp. Med. Biol. 628, 102114.

43. Mazor, O., and Laurent, G. (2005). Transient dynamics versus fixed points in odor representations by locust antennal lobe projection neurons. Neuron 48, 661673.

44. Mercer, A. R., Mobbs, P. G., Davenport, A. P., and Evans, P. D. (1983). Biogenic amines in the brain of the honeybee, Apis mellifera. Cell and tissue research, 234(3), 655-677.

45. Menzel R. and Muller U. (1996) Learning and memory in honeybees: from behavior to neural substrates. Annu. Rev. Neurosci. 19, 379 404.

46. Menzel, R., Heyne, A., Kinzel, C., Gerber, B., and Fiala, A. (1999). Pharmacological dissociation between the reinforcing, sensitizing, and response-releasing functions of reward in honey- bee classical conditioning. Behav. Neurosci. 113, 744754.

47. Meyer, A., and Galizia, C. G. (2012). Elemental and configural olfactory coding by antennal lobe neurons of the honeybee (Apis mellifera). J. Comp. Physiol. A Neuroethol. Sens. Neural. Behav. Physiol. 198, 159171.

48. Mller E (2007) Markov Process Models for Neural Ensembles with Spike-Frequency Adaptation. PhD Thesis, Combined Faculties for the Natural Sciences and for Mathematics.

49. Mller E, Buesing L, Schemmel J, Meier K (2007) Spike-frequency adapting neural ensembles: beyond mean adaptation and renewal theories. Neural Comput 19(11):2958-3010.

50. Nawrot MP (2010) Analysis and interpretation of interval and count variability in neural spike trains. In: Analysis of parallel spike trains, ed. by. S Grn and S Rotter, Springer Series in Computational Neuroscience.

51. Nawrot, M. P., Krofczik, S., Farkhooi, F., and Menzel, R. (2010). Fast dynamics of odor rate coding in the insect antennal lobe.

52. Neher, E. (1971). Two fast transient current components during voltage clamp on snail neurons. Journal of General Physiology 58: 36.

53. Nordstrom, M., Fuglevand, A., and Enoka, R. (1992). Estimating the strength of common input to human motoneurons from the cross- correlogram. J. Physiol., 453:547574.

54. Nishino, H., Nishikawa, M., Mizunami, M., and Yokohari, F. (2009). Functional and topographic segre- gation of glomeruli revealed by local staining of antennal sensory neu- rons in the honeybee Apis mellifera. J. Comp. Neurol. 515, 161180.

55. Olsen, S. R., Bhandawat, V., and Wilson, R. I. (2007a). Excitatory interactions between olfactory processing channels in the Drosophila antennal lobe. Neuron 54, 89103.

56. Peng, I. F., Wu, C. (2007). Differential contributions of Shaker and Shab K+ currents to neuronal firing patterns in Drosophila. Journal of neurophysiology 97: 780.

57. Prescott S, Ratte S, De Koninck Y, Sejnowski T (2008) Pyramidal neurons switch from integrators in vitro to resonators under in vivo-like conditions. Journal of Neurophysiology 100: 3030.

58. Purves D, Augustine GJ, Fitzpatrick D, et al. (2001). Neuroscience. 2nd edition. Sunderland (MA): Sinauer Associates. The Biogenic Amines.

59. Reale V., Hannan F., Midgley J. M., and Evans P. D. (1997) The expression of a cloned Drosophila octopamine/tyramine receptor in Xenopus oocytes. Brain Res. 769, 309 320.

60. Ryglewski, S., Duch, C. (2009). Shaker and Shal mediate transient calcium independent potassium current in a Drosophila flight motoneuron. Journal of Neurophysiology : 006932009.

61. Roeder, T. (2005). Tyramine and octopamine: ruling behavior and metabolism. Annu. Rev. Entomol., 50, 447-477.

62. Robb S, Cheek TR, Hannan FL, Hall LM, Midgley JM, Evans PD. (1994). Agonist-specific coupling of a cloned Drosophila octopamine/ tyramine receptor to multiple second messenger systems. EMBO J. 1994;13:13251330.

63. Rocha, J., Doiron, B., Shea-Brown, E., Josic, K., and Reyes, A. (2007). Correlation between neural spike trains increases with firing rate. Nature, 448:802807.

64. Rush, M., Rinzel, J. (1995). The potassium A-current, low firing rates and rebound excitation in Hodgkin- Huxley models. Bulletin of mathematical biology 57: 899929.

65. Rybak, J., and Menzel, R. (1993). Anatomy of the mushroom bodies in the honey bee brain: the neu- ronal connections of the alpha-lobe. J. Comp. Neurol. 334, 444465.

66. Sachse, S., and Galizia, C. G. (2002). Role of inhibition for temporal and spatial odor representation in olfac- tory output neurons: a calcium imaging study. J. Neurophysiol. 87, 11061117.

67. Saito, M. & Wu, C. (1991). Expression of ion channels and mutational effects in giant Drosophila neurons differentiated from cell division-arrested embryonic neuroblasts. Journal of Neuroscience 11: 2135.

68. Sears, T. and Stagg, D. (1976). Short-term synchronization of intercostal motoneurone activity. J. Physiol., 263:357381.

69. Seki, Y., Rybak, J., Wicher, D., Sachse, S., and Hansson, B. S. (2010). Physiological and morpholog- ical characterization of local interneurons in the Drosophila antennal lobe. J. Neurophysiol. 104, 10071019.

70. Shepherd, G. (1998). The Synaptic Organization of the Brain, Fourth Edition. Oxford University Press, Inc.

71. Shang, Y. H., Claridge-Chang, A., Sjulson, L., Pypaert, M., and Miesenbock, G. (2007). Excitatory local circuits and their implications for olfactory processing in the fly antennal lobe. Cell 128, 601612.

72. Sinakevitch, I. G., Geffard, M., Pelhate, M., and Lapied, B. (1996). Anatomy and targets of dorsal unpaired median neurones in the terminal abdominal ganglion of the male cockroach Periplaneta americana L. J. Comp. Neurol. 367, 147163.

73. Sinakevitch, I., Douglass, J.K., Scholtz, G., Loesel, R., and Strausfeld, N.J. (2003). Conserved and convergent organization in the optic lobes of insects and isopods, with reference to other crustacean taxa. The Journal of comparative neurology 467, 150-172.

74. Sinakevitch, I., Mustard, J.A., and Smith, B.H. (2011). Distribution of the octopamine receptor AmOA1 in the honey bee brain. PloS one 6, e14536.

75. Sinakevitch, I., Niwa, M., and Strausfeld, N.J. (2005). Octopamine-like immunoreactivity in the honey bee and cockroach: comparable organization in the brain and subesophageal ganglion. The Journal of comparative neurology 488, 233-254.

76. Sinakevitch, I., Smith, A., Locatelli, F., Huerta, R., Bazhenov, M. and Smith, B. (2013). Apis mellifera octopamine receptor 1 (AmOA1) expression in antennal lobe networks of the honey bee (*Apis mellifera*) and fruit fly (*Drosophila melanogaster*). Front. Syst. Neurosci. 7:70.

77. Sinakevitch, I., and Strausfeld, N.J. (2004). Chemical neuroanatomy of the fly's movement detection pathway. The Journal of comparative neurology 468, 6-23.

78. Sinakevitch, I., and Strausfeld, N.J. (2006). Comparison of octopamine-like immunoreactivity in the brains of the fruit fly and blow fly. The Journal of comparative neurology 494, 460-475.

79. Sinakevitch, I.G., Geffard, M., Pelhate, M., and Lapied, B. (1996). Anatomy and targets of Dorsal Unpaired Median neurones in the Terminal Abdominal Ganglion of the male cockroach Periplaneta americana L. The Journal of comparative neurology 367, 147-163.

80. Strausfeld, N. J., Sinakevitch, I., and Vilinsky, I. (2003). The mushroom bodies of Drosophila melanogaster: an immunocytological and golgi study of Kenyon cell organiza- tion in the calyces and lobes. Microsc. Res. Tech. 62, 151169.

81. Stocker, R. F., Lienhard, M. C., Borst, A., and Fischbach, K. F. (1990). Neuronal architecture of the antennal lobe in Drosophila melanogaster. Cell Tissue Res. 262, 934.

82. Strausfeld, N.J., Sinakevitch, I., and Vilinsky, I. (2003). The mushroom bodies of Drosophila melanogaster: an immunocytological and golgi study of Kenyon cell organization in the calyces and lobes. Microscopy research and technique 62, 151-169.

83. Strausfeld, N. J. (2002). Organization of the honey bee mushroom body: representation of the calyx within the vertical and gamma lobes. J. Comp. Neurol. 450, 433.

84. Tanaka, N. K., Endo, K., and Ito, K. (2012a). Organization of antennal lobe-associated neurons in adult Drosophila melanogaster brain. J. Comp. Neurol. 520, 40674130.

85. Tanaka, N. K., Suzuki, E., Dye, L., Ejima, A., and Stopfer, M. (2012b). Dye fills reveal additional olfactory tracts in the protocerebrum of wild-type Drosophila. J. Comp. Neurol. 520, 41314140.

86. Tanaka, N. K., Tanimoto, H., and Ito, K. (2008). Neuronal assemblies of the Drosophila mushroom body. J. Comp. Neurol. 508, 711755.

87. Tierney, A., Harris-Warrick, R. (1992). Physiological role of the transient potassium current in the pyloric circuit of the lobster stomatogastric ganglion. Journal of neurophysiology 67: 599.

88. Tsunoda, S., Salkoff, L. (1995). Genetic Analysis of Drosophila Neurons: Shal, Shaw, and Shab Encode Most Embryonic Potassium Currents. Journal of Neuroscience 15: 1741-1754..

89. Walmsley, B., Edwards, F., and Tracey, D. (1988). Nonuniform release probabilities underlie quantal synaptic transmission at a mammalian excitatory central synapse. J. Neurophysiol., 60(3):889908.

90. Weinstock, G. M., Robinson, G. E., Gibbs, R. A., Worley, K. C., Evans, J. D., Maleszka, R., ... and Huybrechts, J. (2006). Insights into social insects from the genome of the honeybee Apis mellifera. Nature, 443(7114), 931-949.